258

STUDY OF COMPATIBILITY AND ASYMMETRY IN CAR-TO-CAR IMPACTS

by

B. Samuel Holmes and James K. Gran

Supervisor
James D. Colton

STANFORD RESEARCH INSTITUTE
333 RAVENSWOOD AVENUE
MENLO PARK, CALIFORNIA 94025

August 1975

Interim Report
Contract No. DOT-TSC-843
SRI Project PYU-3578

Prepared for:

U.S. DEPARTMENT OF TRANSPORTATION
NATIONAL HIGHWAY TRAFFIC SAFETY ADMINISTRATION
WASHINGTON, D.C. 20590

Prepared for the Department of Transportation, National Highway Traffic Safety Administration under Contract No. DOT-TSC-843. The opinions, findings, and conclusions expressed in this publication are those of the authors and not necessarily those of the National Highway Traffic Safety Administration.

Technical Report Documentation Page

1. Report No.	2. Government Accession No.	3. Recipient's Catalog No.

4. Title and Subtitle	5. Report Date
STUDY OF COMPATIBILITY AND ASYMMETRY IN CAR-TO-CAR IMPACTS	August 1975
	6. Performing Organization Code: SRI Project PYU-3578
7. Author(s): B. Samuel Holmes and James K. Gran Supervisor: James D. Colton	8. Performing Organization Report No.: Interim Report
9. Performing Organization Name and Address: Stanford Research Institute 333 Ravenswood Avenue Menlo Park, California 94025	10. Work Unit No. (TRAIS) 11. Contract or Grant No.: DOT-TSC-843
12. Sponsoring Agency Name and Address: U.S. Department of Transportation National Highway Traffic Safety Administration Washington, D.C. 20590	13. Type of Report and Period Covered: Interim Report 14. Sponsoring Agency Code

15. Supplementary Notes

16. Abstract

Analyses and scale model experiments are used to investigate the structural characteristics that make large and small vehicles compatible in frontal impacts. The first half of the study, described in this report, includes an analysis of the compatibility of three existing safety vehicles in in-line frontal impacts and new designs of a subcompact and a full-size car for increased compatibility. These new designs are tested in a series of scale model experiments. Interpretation of the experiments in terms of occupant response is facilitated with a one degree-of-freedom analytical model of an occupant and airbag restraint system. It is concluded that subcompact to full-size cars can be made to provide survivable accelerations in both to mph frontal barrier and 80 mph frontal car-to-car impacts.

In addition to the study of compatibility, the utility of scale models in the study of automobile sheet metal response was also investigated. A 1/5th scale model of the front-end sheet metal of a full-size car was built and tested in a barrier impact. Comparison of the scale model test with a corresponding full-scale test shows that this type of structure can be modeled accurately.

17. Key Words	18. Distribution Statement
Crash worthiness Compatibility Scale-model Structures Energy Absorption	

19. Security Classif. (of this report)	20. Security Classif. (of this page)	21. No. of Pages	22. Price
UNCLASSIFIED	UNCLASSIFIED	104	

Form DOT F 1700.7 (8-72) Reproduction of completed page authorized

CONTENTS

CONTENTS (Concluded)

ILLUSTRATIONS

ILLUSTRATIONS (Concluded)

TABLES

I INTRODUCTION

The two primary objectives of this study are to find the structural characteristics that make large and small vehicles more compatible in car-to-car impacts and to demonstrate experimentally that such structures can be built within the size and weight range of current cars. A secondary objective is to extend scale modeling techniques (Reference 1) to include automotive sheet metal structures. The scale model experiment is the chief experimental tool in this work.

This report describes the first part of the compatibility study: the analytical and experimental investigation of the compatibility of front-engined vehicles weighing from 2500 to 4500 pounds in head-on car-to-car impacts and barrier impacts. The scale modeling of an automobile sheet metal structure is also discussed.

Background

Most injuries in high speed traffic accidents result from excessive occupant accelerations or from occupant contact with the car interior. The occupant acceleration history depends on the occupant restraint system and the crush characteristics of the structure. The severity of occupant impact with the car interior depends on occupant motion and intrusion of the car structure into the passenger compartment. Thus the degree of occupant injury is determined by the restraint

---

[1] B. S. Holmes and G. E. Sliter, "Methods, Application and Cost Effectiveness of Scale Model Studies of Automobile Impacts," Stanford Research Institute Final Report (September 1974). Available from the National Technical Information Service, DOT HS-801-233.

system and by the response of the vehicle structure to which the restraint system is attached. The structural response and subsequent restraint and occupant response are in turn a complex function of the object struck as well as the impact angle, velocity, and contact point.

Most serious injuries and fatalities in automobile accidents occur in frontal and oblique frontal impacts with fixed obstacles at speeds to 50 mph and with other cars at closure speeds to 80 mph. Clearly, the vehicle structure/restraint systems in use today must be improved to assure occupant safety at these speeds. This is especially true in smaller cars, which have less crush space and undergo larger accelerations in collisions with large cars (Reference 2).

When the occupants of one vehicle are likely to suffer serious injuries in a specified collision with a second vehicle, the vehicles are said to be "incompatible" in that collision. The problem of structural compatibility between large and small vehicles is aggravated by the relative stiffness or crush strength of the vehicles. Large cars are proportionately stiffer than small cars. Although this difference in stiffness is beneficial in collisions with fixed objects, it is detrimental in collisions between large and small cars because most of the resultant deformation occurs in the small car. Thus, to assure compatibility, it is not enough to change one vehicle type; the entire vehicle system should be improved to assure maximum compatibility between large and small vehicles in car-to-car impacts as well as acceptable performance in barrier impacts.

---

[2] J. Hofferberth and J. Tomassoni, "A Study of Structural and Restraint Requirements for Automobile Crash Survival," presented at the 3rd International Congress on Automotive Safety by the National Motor Vehicle Safety Advisory Council (July 1974).

The feasibility of making dramatic improvements in compatibility for in-line frontal impacts has been shown by Hofferberth and Tomassoni (Reference 2) in an analytical study of the effect of modifying both structure and restraint systems of current cars without changing their weight or length. In this study a variety of restraint system and structure options were investigated to find the range of vehicle sizes and velocities where compatibility is possible. It was concluded that a significant improvement in structural compatibility can be achieved by changing the front-end stiffness and engine location and by increasing the allowable engine displacement to provide more crush. However, although the stiffness of the system of vehicles was varied in this study, the shape of the force-deflection curves of the vehicles was always a linearly increasing function followed by collapse at a constant force.

Scope and Objectives

The scope of the current program is limited to the impacts that cause the most injuries and fatalities: frontal impacts with fixed objects or barriers and frontal impacts between two vehicles. Both symmetric and asymmetric (angular) impacts are included, but side and rear impacts are not. The scope is further limited to front-engined vehicles weighing between 2500 and 4500 pounds, i.e., current subcompact to full size cars.

The three objectives of the program are to:

(1) Determine force-deflection characteristics for the front structures of subcompact to full size vehicles that will assure occupant safety in 50-mph frontal barrier impacts and in 80-mph car-to-car impacts. Since the structure and occupant restraints form a system that determines occupant safety, an appropriate restraint system must also be recommended for the vehicles.

(2) Demonstrate with scale model experiments that the desired structural performance can be achieved with vehicles of the size and weight of current cars.

(3) Develop scale modeling techniques for studying the response of automobile sheet metal in high speed impacts.

The study of compatibility was divided into two parts; in-line impacts were studied first and angular impacts second. This report describes the work on in-line impacts and the scale modeling of automobile sheet metal.

Approach

The study of in-line frontal impacts was conducted by the following approach. First, relatively simple structural and restraint system analyses were combined to evaluate conceptual solutions to the problem of compatibility. Scale model structures based on the best concepts found in the analyses were then designed and tested. Finally, analytical models of restraint systems were used to interpret the experiments. Scale modeling was extended to sheet metal structures by making a direct comparison between the response of a full-scale sheet metal structure with the response of the corresponding scale model structure.

The program to date was broken into five tasks:

(1) Develop analytical models for airbag and belt restraint systems to interpret structural response in terms of occupant safety.

(2) Analytically determine the compatibility in frontal impacts of three existing safety vehicles. These vehicles, developed independently, provide a baseline of compatibility for vehicles designed for barrier impacts.

(3) Based on the restraint and compatibility analyses, design a system of subcompact and full size vehicles with increased compatibility in frontal impacts.

(4) Test the design concepts developed in Task 3 in scale model experiments of frontal barrier and car-to-car impacts.

(5) Extend the scale modeling technique to include automotive sheet metal.

Each of these tasks is discussed in more detail in the following subsections.

Task 1--Restraint System Analysis

Two restraint systems, an airbag and seat belts, were mathematically modeled in this study. In the initial analysis of the models, it was found that a belt system imposes severe demands on structural performance because of the low human tolerance to acceleration of a belted occupant. An airbag system yields far better overall results because the higher limits of human tolerance to acceleration for an occupant supported by an airbag result in less severe demands on structural performance. Consequently, only the airbag restraint system was developed and studied in detail.

The mathematical model for an airbag restraint system consists of an airbag mounted on a crushable, constant-force bolster. The occupant is modeled as a single mass with one degree of freedom. This analytical model was incorporated into a computer program that predicts occupant response for a given acceleration history or "crash pulse" of the passenger compartment. The program was used first to find the envelope of acceptable occupant compartment crash pulses and then to evaluate crash pulses measured in experiments.

Task 2--Compatibility Analysis of Minicars, AMF, and Calspan Vehicles

These three vehicles were developed independently to standards that improve safety in barrier impacts. Each vehicle meets or nearly meets criteria for survivability in 50-mph barrier impacts. These safety vehicles encompass the range of vehicle sizes (subcompact to full size) included in the study reported here, and provided a baseline of compatibility. The compatibility of these vehicles with each other was studied with an analytical model that represents each vehicle as a series of masses connected by nonlinear springs. The accuracy of the model was tested by using it first to predict vehicle response in barrier impacts and then comparing this response with full-scale experiments from the vehicle development program. When satisfactory correlation was obtained, the analytical model was used to predict performance in car-to-car impacts of the three safety vehicles.

Task 3--Design of More Compatible Vehicles

The analysis of the Minicars, AMF, and Calspan vehicles was used to point out features of the vehicles that could be altered to increase compatibility. New designs were developed with the aid of the mass-spring analysis. This part of the study was limited to two vehicle sizes, a subcompact and a full-size vehicle, because the concepts used in these designs could be used for the entire range of vehicle sizes within the scope of this study.

One-fifth scale model structures with the force-deflection characteristics determined in the analysis were then designed for the two-vehicle system. Both vehicles used a foam filled aluminum front structure similar to that developed by Minicars because this was the simplest method of obtaining the desired stiffness characteristics.

Task 4--Compatibility Experiments

A model of Minicars' subcompact foam nose was dynamically tested and its crush characteristics compared with those obtained by Minicars in full-scale tests to show that scale models of foam filled vehicles accurately reproduce the response of the corresponding full-scale structures. Then a scale model of the Minicars design with complete front end was tested in a 50-mph barrier impact and compared with a corresponding full-scale test by Minicars.

The improved vehicles designed in Task 3 were then tested with scale model experiments. Two scale model experiments were performed to verify the designs of the full size car: a 50-mph barrier test and a car-to-car test to demonstrate the compatibility of the two vehicles in head-on impacts at 77 mph.

Task 5--Extending Scale Modeling Techniques to Include Sheet Metal Structures

An explosive forming technique was used to make complex sheet metal parts in a 1/5-scale model of a 1968 Plymouth sheet metal front end. The model was tested in a 19-mph barrier impact reproducing a similar full-scale test (Dynamic Science Test 289-49, Reference 3). The response observed in the model was compared with that observed in the full-scale test on the basis of high speed movies, accelerometer data, and postcrash inspection.

---

[3] S. M. Shaw, A. D. Harper, and R. L. Anderson, "Vehicle Front End Structure Crash Evaluation Program, Volumes I, II, and III," Dynamic Science Final Report (May 1974). Available from the National Technical Information Service, DOT-HS-046-2-486.

Report Organization

The remainder of the report is divided into five sections. A summary of key findings and the conclusions reached is given in Section II. The restraint system analysis is described in Section III. The frontal impact analysis of the Minicars, AMF, and Calspan vehicles and the design of improved vehicles are presented in Section IV, and the validation of the analysis with scale model experiments is described in Section V. The development of techniques to model automotive sheet metal and the comparisons of a 1/5-scale test and a full-scale test are given in Section VI. A supplementary description of the mass-spring analysis of vehicles and the data used in the analyses discussed here are given in Appendices A and B.

II SUMMARY AND CONCLUSIONS

The analyses and experiments described here point the way to the design of subcompact and full-size automobile structures with improved performance in frontal barrier impacts at speeds up to 50 mph and in car-to-car impacts at speeds up to 80 mph. To date we have found three characteristics that improve structural compatibility and barrier impact performance. These are:

(1) The principal energy absorbing elements in frontal impacts should interact directly with the vehicle body, but not with the engine and transmission.

(2) A system of stepped force-deflection curves yields the best overall barrier and head-on car-to-car impact performance. The force level and duration of each step depends on vehicle weight, the tolerable deviation from "ideal" barrier performance (defined as constant acceleration in a barrier impact), and the closure speed at which car-to-car compatibility is desired.

(3) The best front-end energy management systems are those that absorb energy through large changes in the volume of the vehicle; systems that rely on bumper alignment are less desirable.

Extension of the scale modeling technique to include automotive sheet metal has provided an economical and accurate alternative to numerical methods and full-scale experiments for the study of large deformations of sheet metal structures.

These conclusions were reached as a result of the work performed to date on each of the five tasks described in the Introduction. This work is summarized by task below.

Restraint System Analysis

Analytical models of occupant response were developed for an airbag/crushable bolster restraint system and for a force-limited belt system. For both systems the occupant was modeled as a single mass with one degree of freedom. Thus the analytical models gave realistic estimates of restraint performance in controlling torso motion but not head and limb motion. We can now predict injury to the occupants when it is a result of the occupant acceleration history as measured by the chest severity index (CSI), rate of onset of acceleration (jerk), excessive occupant translation in the passenger compartment (stroke), and final occupant velocity. Since head and limb motion may also affect occupant injury, the restraint analyses gave upper bounds on restraint performance.

The analytical restraint system models were incorporated into a computer program (BOUNCE), which simulates occupant response to a given passenger compartment acceleration history, or crash pulse. Initial analysis of the belt system indicated that it would be very difficult to meet the compatibility requirements with that system. Consequently, only the airbag system was used to evaluate structural response in further analyses and experiments.

The airbag system parameters were then optimized for an occupant compartment crash pulse with a nearly rectangular* shape for impact speeds from 20 to 50 mph. Other crash pulses were analyzed with the BOUNCE program to determine the restraint system's tolerance to changes in pulse shape. It was found that the airbag system has significant tolerance to variations in the shape and duration of the crash pulse but that any change from those for which the system is designed results in a decrease in performance.

---

*An occupant compartment acceleration history characterized by a sharp rise followed by a constant acceleration until forward motion stops.

Compatibility Analysis of Minicars, AMF, and Calspan Vehicles

The compatibility of these three vehicles was analyzed with a computer program (COMPAT), which models the vehicle as a system of masses connected by nonlinear springs. Similar analyses have been used extensively in the past (Reference 3) to show how various features of a vehicle structure affect its crash response. This type of analysis requires prior knowledge of the major sections of the vehicle that will deform and the force-deflection characteristics of these sections. The mass and spring characteristics for the three safety vehicles were developed from information published by their designers (References 4, 5, and 6). The accuracy of the analytical models was then tested by comparing the responses predicted by the COMPAT program with those observed in previous full-scale 50-mph barrier tests on these vehicles.

The responses of these three vehicles in car-to-car impacts at 70 and 80 mph closure speeds were then calculated with the COMPAT program. These analyses led to two conclusions affecting the design of new vehicles in this study. First, the Minicars, AMF, and Calspan vehicles were not compatible at 70-80 mph closure speeds since the occupant acceleration histories predicted by the restraint analysis were not survivable. Second, of these three vehicles, the response of the Minicars vehicle was least dependent on the crush properties of the struck vehicles and was most similar in barrier impacts and impacts with the other vehicles.

---

[4] P. M. Miller and J. E. Greene, "Development and Evaluation of a Structural Crashworthiness System for a Standard Size Automobile," Calspan Corporation Final Report (June 1974), DOT-HS-053-2-487.

[5] W. J. Wingenbach and R. E. Lagerquist, "Frontal and Side Impact Crashworthiness--Compact Cars," AMF Incorporated Final Report (March 1974). Available from the National Technical Information Service, DOT-HS-257-2-461.

[6] Private Communication with Minicars, Inc., of Goleta, California.

This characteristics of the Minicars vehicle is a result of the vehicle design, which uses foam filled sheet metal as a major energy absorbing element. This design provides different load paths for decelerating the body and the engine, minimizing the interaction of the engine and body motions. Also, since the foam absorbs energy through large changes in volume, problems of misalignment are minimized. Of course, other structures that absorb energy by large volume changes (e.g., aluminum honeycomb) could be used to obtain these structural characteristics.

Design of More Compatible Vehicles

As a result of the observations made in Task 2, we designed a new vehicle system (consisting of a subcompact and a full-size vehicle) using foam filled sheet metal as the principal energy absorbing element. The basic design philosophy used in developing the two-vehicle system is as follows. The small car uses all its crush space in a 50-mph barrier impact by crushing at a nearly constant force, which produces a nearly rectangular 30-g crash pulse. The front of the large car is made with a two-step force level and consequently produces a stepped crash pulse. The first force level is the same as that of the small car, and the second force level is chosen to limit peak acceleration of the large car to 35 g in a 50-mph barrier crash. The crush distances at each force level are chosen so that the large car uses its entire crush distance in a 50-mph barrier crash. Thus the barrier performance of the large car is compromised to make its structure more compatible with that of the small car.* An intermediate size car would also be designed with a two-step force level, but the location of the stiffness change and the level of the second step would depend on the vehicle's weight and dimensions.

---

*If a side impact criteria were also included in the design of the vehicle system, a third and softer step would be included in the front of all the vehicles including the smallest one.

These criteria were used to design front structures for a subcompact and full size car. Both designs used urethane foam enclosed in an aluminum shell. The subcompact design was similar to Minicars' original subcompact vehicle. The full size design incorporated the same concepts, but included the stepped force levels. The 1/5-scale models of the vehicles constructed to prove the feasibility of the designs are shown in Figure 1. The change in force level in the full size vehicle was obtained by the change in cross sectional area of the foam structure seen in the vehicle on the left.

Compatibility Experiments

Scale models of both vehicles were tested in barrier impacts at 50 mph and in a head-on car-to-car impact at 77 mph. The high speed movies and accelerometer data taken during the barrier tests were used to compare vehicle response with that predicted by the COMPAT analysis, and showed that the designs performed as desired. Vehicle performance in the 77-mph two-car test was also similar to that predicted by analysis. Figure 2 shows the occupant compartment accelerations of the two vehicles measured in this test. Note that both crash pulses are nearly rectangular, as desired. Analysis of the crash pulses with the occupant restraint model indicated that the response of both vehicles fell within the range of desired response in all these tests.

Scaled Sheet Metal Structures Experiments

In this task, a dynamic test of the front end sheet metal of a full-scale 1968 Plymouth was compared with a corresponding 1/5-scale model test. The objective of the full-scale test was to measure the force-deflection characteristics, and thereby, the energy absorbing capacity, of automobile front end sheet metal. The objective of the model test was to assess the utility of scale modeling for investigating

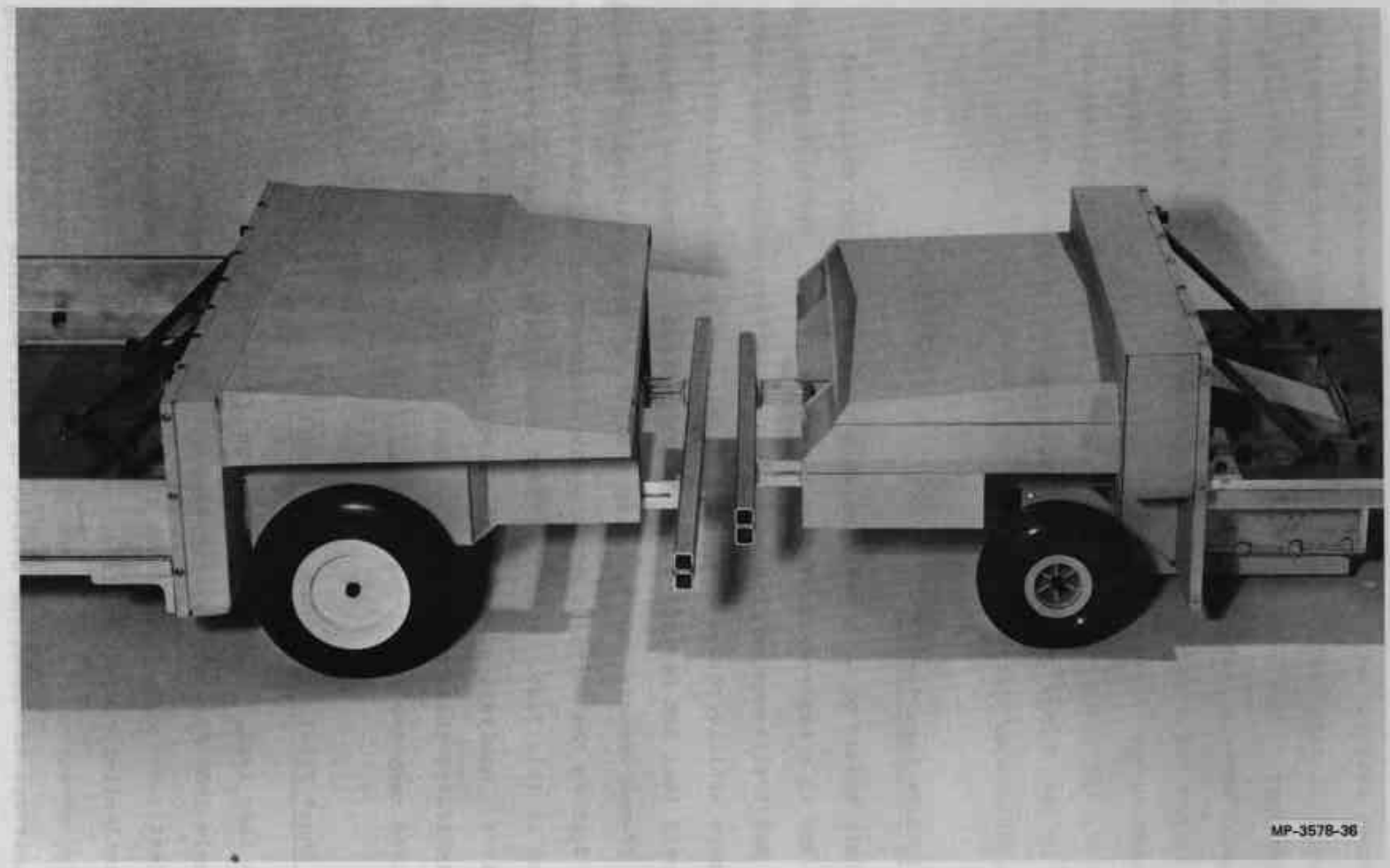

FIGURE 1 1/5-SCALE MODELS OF FULL SIZE (LEFT) AND SUBCOMPACT (RIGHT) VEHICLES

These vehicles are compatible in 80-mph car-to-car frontal impacts and retain 50-mph barrier performance.

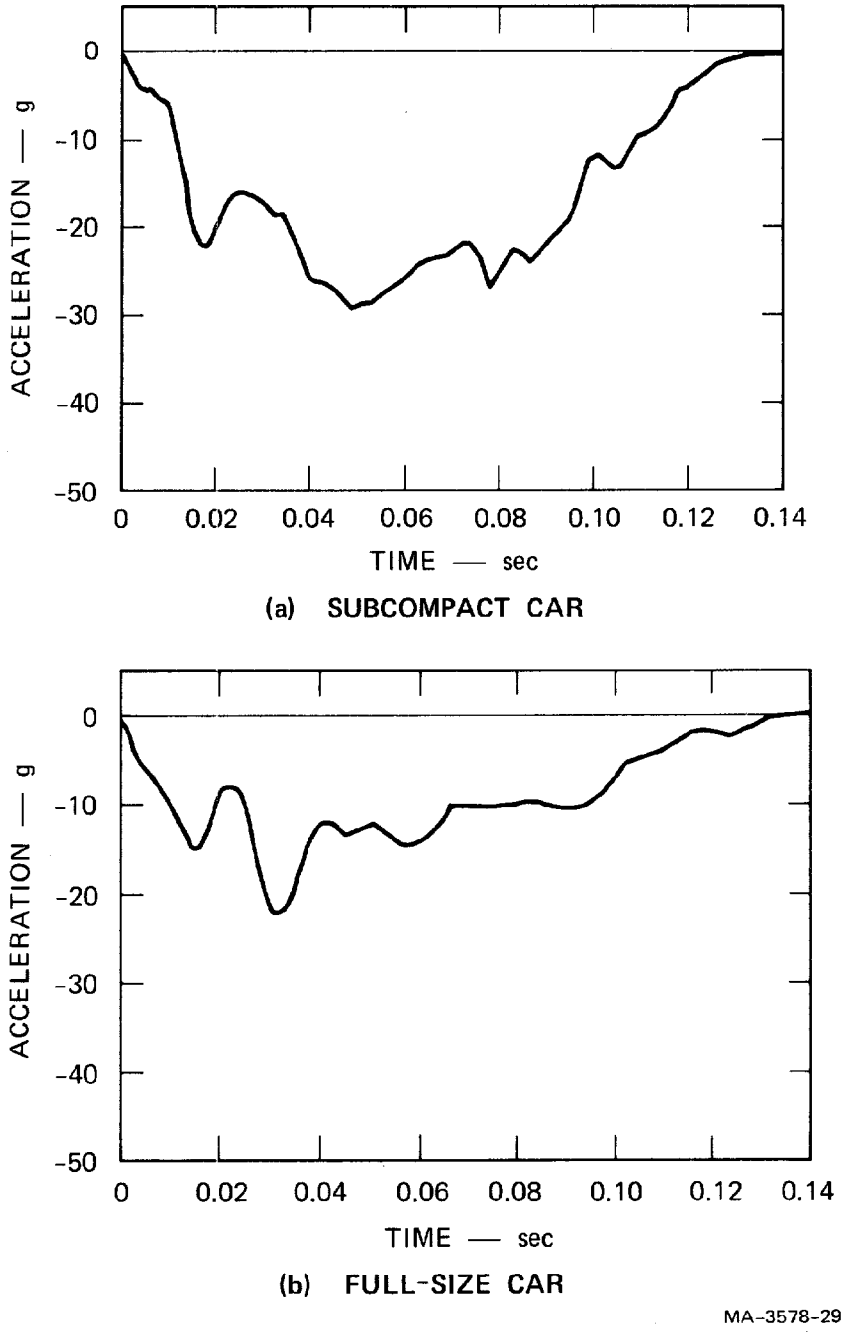

FIGURE 2 LONGITUDINAL PASSENGER COMPARTMENT ACCELERATIONS FOR SUBCOMPACT (TOP) AND FULL SIZE (BOTTOM) SCALE MODEL VEHICLES IN 77-mph FRONTAL IMPACT TEST

sheet metal structures. In the full-scale test performed by Dynamic Science (Reference 3), the engine, frame, bumper, and front suspension were removed from the test vehicle. The remaining body and front end sheet metal were tested in a 20-mph barrier impact. Vehicle crush and acceleration were then used to estimate the sheet metal force-deflection characteristics. The 1/5-scale model vehicle was built and tested by SRI.

The critical step in model construction was in forming sheet metal parts with compound curves and a thickness of only 0.007 inch. An explosive forming process adaptable to many shapes of parts was used to fabricate the components of the sheet metal model. Overall dimensions of the model were within 2 percent of scaled dimensions of a full-scale vehicle, and sheet metal thicknesses in the model were within 5 percent of corresponding scaled thicknesses of the full-scale Plymouth. The yield strength and ultimate strength of the sheet metal in the model were about 10 percent greater than in the full-scale vehicle.

When the movies and acceleration histories from the full-scale and 1/5-scale tests were compared, it was found that the overall response was similar in both. The high speed movies showed that the sheet metal noses "rolled" under and the vehicles pitched upward. The accelerometer measurements from the two experiments were similar, indicating that the initial strength of the sheet metal decreased rapidly when it rolled under. The peak accelerations in the two tests differed by 13 percent, and the dynamic crush differed by 41 percent. These differences are attributed to the differences in sheet metal yield stress and scaled thickness of the full-size and scale model sheet metal components.

Conclusions and Recommendations

Three major conclusions resulted from this study.

(1) The structures of cars ranging from subcompact to full size can be made to provide survivable accelerations in frontal car-to-car impacts up to 80 mph. Restraint systems in these vehicles must be tailored to the structural characteristics of the vehicles.

(2) The performance of safety vehicle structures can be improved by including three characteristics in their design; (a) principal energy absorbing elements that interact directly with the body, (b) a system of stepped force-deflection characteristics keyed to the smallest car, and (c) energy absorption through large changes in volume.

(3) The scale modeling technique can be extended to include automotive sheet metal.

The objective of future work will be to extend the conclusions for structural response in in-line barrier and car-to-car impacts to include general asymmetric impacts. As in the barrier and car-to-car impacts, structural performance in one impact mode may have to be sacrificed for improvement in another mode. These compromises can be based on the relative frequency and societal cost of different types of accidents.

III RESTRAINT SYSTEM ANALYSIS

The purpose of the analysis of restraint systems was twofold: first, to find constraints on "acceptable" structural performance, and second, to interpret in terms of occupant response the crash pulses measured in the scale model experiments. The restraint analysis was not intended to rank structural performance beyond satisfactory or unsatisfactory, but to determine for a particular structure whether an impact is survivable with a suitable restraint system.

Mathematical models were developed for a seat belt restraint system and an airbag system. The belt system was found unsuitable as summarized below. The model of the airbag was made to represent a restraint system that is tolerant of changes in crash pulse shape, yet has characteristics, such as deployment time, that are within the state of the art. This model was incorporated into a computer program (BOUNCE), which calculates occupant response and predicts the level of injury in terms of the chest severity index (CSI), rate of onset of acceleration, and other parameters as described in detail in this section.

Seat Belt System Model

A simple mathematical model of a seat belt restraint system was analyzed to determine the demands of this type of restraint system on vehicle structural performance. In the model, the occupant was treated as a single mass with one degree of freedom. The belts were considered elastic-plastic, and both the shoulder belt and lap belt were inclined 45^{o} to the horizontal. The belt characteristics were chosen so that the occupant experienced the human tolerance limits for jerk and peak acceleration with belt systems.

Predicted response of this system to a variety of crash pulses indicated that force limiting belts allowed too much occupant displacement. It was concluded that the use of belt systems would result in significantly lower acceptable impact velocities.

Mathematical Model of Airbag System

Because the airbag restraint system with a crushable bolster was anticipated to have a high tolerance for variations in the occupant compartment acceleration pulse, the model of this system was developed in detail. Figure 3 is a schematic of the airbag and the crushable bolster support mounted in the occupant compartment.

Geometric Relations

The purpose of this analysis is to calculate the response of the occupant $x_1(t)$ given the motion of the occupant compartment $x_2(t)$. The translation of the airbag-bolster interface relative to the occupant compartment is $x(t)$ as shown in Figure 3 and the occupant's displacement relative to the airbag/bolster interface as $S(t)$ is

$$S(t) = x_1(t) - x_2(t) - z(t) \tag{1}$$

The initial clearance between the occupant and the fully inflated bag is designated S_c and the airbag crush is, then, $S - S_c$. The maximum occupant stroke is D and the thickness of the crushable bolster is B.

The rate of gas flow $C(t)$ into the airbag is a delayed step function with a finite duration given by the equations

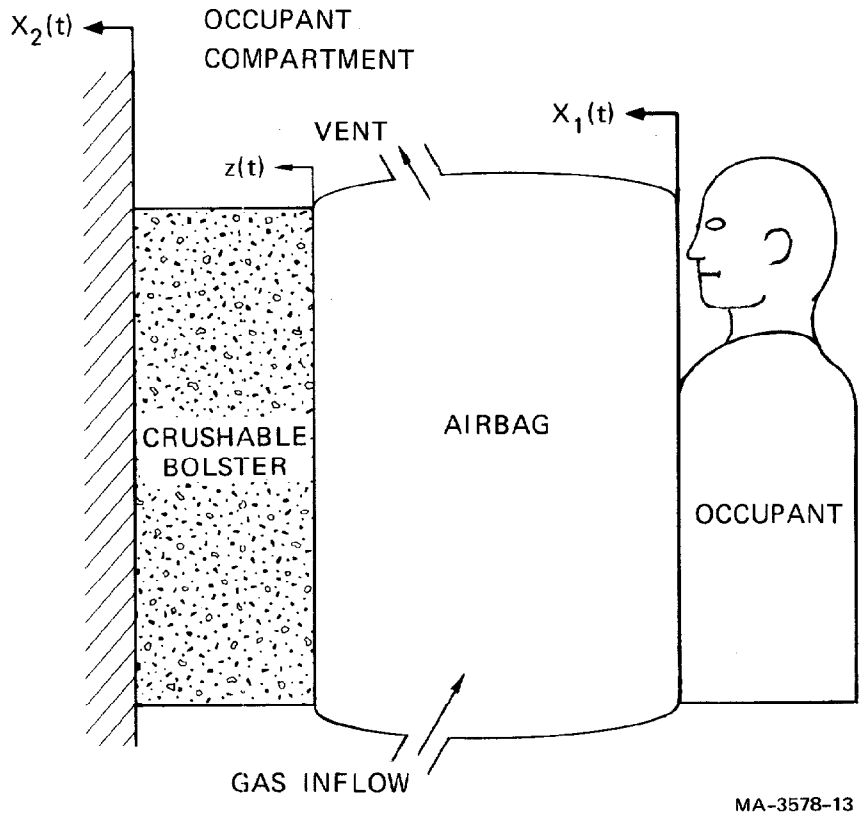

FIGURE 3 SCHEMATIC OF AIRBAG/BOLSTER RESTRAINT MODEL

$$C(t) = 0 \quad \text{when} \quad 0 \le t < t_{on}$$

$$C(t) = C_o \quad \text{when} \quad t_{on} \le t \le t_{off} \tag{2}$$

$$C(t) = 0 \quad \text{when} \quad t > t_{off}$$

The relations for airbag volume and airbag/occupant contact area versus crush are specified as simple functions that approximate a realistic airbag design. The volume V of the airbag is constant until the occupant contacts the airbag at $S = S_c$ and then decreases linearly with displacement S from the full volume V_1 to a minimum volume V_2 at $S = S_v$, then remains at V_2. Thus:

$$V(S) = V_1 \quad \text{when} \quad 0 \le S \le S_c$$

$$V(s) = V_1 + \frac{V_2 - V_1}{S_v - S_c}(S - S_c) \quad \text{when} \quad S_c < S \le S_v \tag{3}$$

$$V(s) = V_2 \quad \text{when} \quad S_v < S$$

The occupant contact area A increases linearly with airbag crush to a maximum A_f at $S = S_f$ as given by:

$$A(S) = 0 \quad \text{when} \quad 0 \le S \le S_c$$

$$A(S) = \frac{A_f}{S_f - S_c}(S - S_c) \quad \text{when} \quad S_c < S \le S_f \tag{4}$$

$$A(S) = A_f \quad \text{when} \quad S_f < S$$

Governing Equations

In addition to the airbag's geometric relations, the equations governing the gas flow out of the bag and the motion of the occupant are needed to predict the response of the occupant and airbag system.

The mass flow rate of gas through the airbag vent is given by

$$f(t) = \beta Y A_v \sqrt{24\ P(t)\ \rho(t)} \tag{5}$$

where β is a flow factor depending on the vent shape (for a circular vent, β is 0.9); A_v is the vent area; $P(t)$ and $\rho(t)$ are the internal gauge pressure and gas density, respectively; and

$$Y \equiv \sqrt{\frac{\left(\frac{\gamma}{\gamma - 1}\right)\left(\frac{14.7}{\bar{P}}\right)^{\frac{2}{\gamma}}\left(1 - \frac{14.7}{\bar{P}}\right)^{\frac{\gamma-1}{\gamma}}\left(1 - \bar{R}^4\right)}{\left(1 - \frac{14.7}{\bar{P}}\right)^{\frac{1}{\gamma}}\left[1 - \bar{R}^4\left(\frac{14.7}{\bar{P}}\right)^{\frac{2}{\gamma}}\right]}}$$

where γ is the ratio of specific heats for the gas; $\bar{P}$ is the absolute internal pressure (i.e., $\bar{P} = P + 14.7$ psig); and $\bar{R}$ is the ratio of the vent radius to the airbag equivalent radius (the radius of a sphere having the same volume as the airbag).

Conservation of mass requires that

$$\dot{\mu} = C(t) - f(t) \tag{6}$$

where μ is the mass of gas in the airbag and the dot indicates the derivative with respect to time. Changes in the mass of gas must be accompanied by changes in airbag volume and gas density as given by

$$\dot{\mu} = \frac{d}{dt}(\rho V) = V\dot{\rho} + \rho\dot{V} \tag{7}$$

The derivatives $\dot{\rho}$ and $\dot{V}$ are now evaluated. If the gas flow is assumed to be adiabatic,

$$\rho(t) = \left(\frac{\bar{P}(t)}{\bar{P}(0)}\right)^{\frac{1}{\gamma}} \rho(0) \tag{8}$$

Differentiating equation (8) with respect to time gives

$$\dot{\rho} = \frac{1}{\gamma} \frac{\rho(t)}{\bar{P}(t)} \dot{P} = \frac{1}{\gamma} \rho(0) \bar{P}(0)^{-\frac{1}{\gamma}} \bar{P}(t)^{\frac{1}{\gamma}-1} \dot{P} \tag{9}$$

$$= K\bar{P}^{\frac{1}{\gamma}-1} \dot{P}$$

Also, $\dot{V}$ is evaluated by differentiating equations (3) and (1)

$$\dot{V} = 0 \quad \text{when } 0 \leq S \leq S_c$$

$$\dot{V} = \frac{\dot{V}_2 - V_1}{S_v - S_c} \dot{S} \quad \text{when } S_c < S \leq S_c \tag{10}$$

$$\dot{V} = 0 \quad \text{when } S_v < S$$

Equations (5), (6), (7), (9), and (10) give the equation of state for the system in terms of airbag pressure.

$$V_1 K\bar{P}^{\frac{1}{\gamma}-1}\dot{P} - C(t) + \beta Y A_v\sqrt{24K\,P\bar{P}^{\frac{1}{\gamma}}} = 0 \quad \text{when} \quad 0 \le S \le S_c$$

$$\left[V_1 + \frac{V_2 - V_1}{S_v - S_c}\left(S - S_c\right)\right] K\bar{P}^{\frac{1}{\gamma}-1}\dot{P} + \frac{V_2 - V_1}{S_v - S_c}\dot{S}K\gamma\bar{P}^{\frac{1}{\gamma}}$$

$$- C(t) + \beta Y A_v\sqrt{24K\,P\bar{P}^{\frac{1}{\gamma}}} = 0 \quad \text{when} \quad 0 \le S \le S_c \qquad (11)$$

$$V_2 K\bar{P}^{\frac{1}{\gamma}-1}\dot{P} - C(t) + \beta Y A_v\sqrt{24K\,P\bar{P}^{\frac{1}{\gamma}}} = 0 \quad \text{when} \quad S_v < S$$

Solving for $\dot{P}$,

$$\dot{P} = \frac{C(t) - \beta Y A_v\sqrt{24K\gamma P\bar{P}^{\frac{1}{\gamma}}}}{V_1 K\bar{P}^{\frac{1}{\gamma}-1}} \quad \text{when} \quad 0 \le S \le S_c$$

$$\dot{P} = \frac{C(t) - \beta Y A_v\sqrt{24K\gamma P\bar{P}^{\frac{1}{\gamma}}} - \frac{V_2 - V_1}{S_v - S_c}\dot{S}K\gamma\bar{P}^{\frac{1}{\gamma}}}{V_1 + \frac{V_2 - V_1}{S_v - S_c}(S - S_c)K\bar{P}^{\frac{1}{\gamma}-1}} \quad \text{when} \quad S_c < S \le S_v \qquad (12)$$

$$\dot{P} = \frac{C(t) - \beta Y A_v\sqrt{24K\gamma P\bar{P}^{\frac{1}{\gamma}}}}{V_2 K\bar{P}^{\frac{1}{\gamma}-1}} \quad \text{when} \quad S_c < S$$

The force F on the occupant is

$$F = PA \qquad (13)$$

where A is the contact area given by equation (4). The equation of motion is then

$$
\begin{aligned}
m\ddot{x}_1 &= 0 && \text{when } 0 \le S \le S_c \\
m\ddot{x}_1 &= P \frac{A_f}{S_f - S_c} (S - S_c) && \text{when } S_c < S \le S_f \\
m\ddot{x}_1 &= PA_f && \text{when } S_f < S
\end{aligned}
\tag{14}
$$

The solution of differential equations (12) and (14) is carried out by forward integration with a fourth-order Runge-Kutta scheme. As long as the force on the occupant remains below the crush force of the bolster, $\dot{Z} = 0$ and equations (12) and (14) can be integrated directly.

When the occupant force reaches F_c, the bolster begins to crush, and the occupant force remains at F_c. The equation of motion for the occupant then becomes

$$m\ddot{x}_1 = F_c \tag{15}$$

When this happens the requirement on P for equilibrium is

$$F = \frac{F_c}{A} \tag{16}$$

and consequently

$$\mu = \rho V = K\gamma V \bar{P}^{\frac{1}{\gamma}} \tag{17}$$

Equations (3), (4), (16), and (17) can be solved iteratively for P, A, V, and Z. Eventually, these equations will have no solution in the range of acceptable values for Z. Physically, this corresponds to

one of two conditions. The first case occurs when the force on the occupant drops below F_c. The second case occurs when the bolster is totally crushed and the airbag pressure is no longer limited by equation (16). In either case, pressure is found by integrating (12) with $\dot{Z} = 0$.

Human Tolerance Limits

Once the occupant's motion is determined, several criteria are applied to measure the occupant's likelihood of death or serious injury. The criteria used here are peak acceleration, the rate of onset of acceleration, maximum displacement, final velocity relative to the passenger compartment, and the chest severity index (CSI), which is computed from the occupant's acceleration history, $x_1(t)$, as follows

$$CSI = \int_{t_0}^{t_{final}} x_1(t)^{2.5} dt \qquad (18)$$

The human tolerance limits for peak acceleration, rate of onset, and CSI used here were taken from Reference 2 and are tabulated in Table 1. Note that limits were also placed on maximum displacement of the occupant in the passenger compartment and his residual velocity when the occupant/restraint system interaction ends.

Table 1

OCCUPANT SURVIVAL CRITERIA USED IN AIRBAG RESTRAINT MODEL

Criterion	Limiting Value
Peak acceleration	60 g
Rate of onset	3000 g/sec
CSI	1000
Maximum displacement	24 inches
Residual velocity	-25 ft/sec < RV < 10 ft/sec

In the analysis of experimental data presented in this report, measured longitudinal acceleration from the scale model experiments is scaled up to full scale and then used as input to the restraint analysis code. It is assumed that each of the five criteria in Table 1 must be met for structural performance in the scale model experiment to be labeled satisfactory. The five criteria are considered equally important.

Optimum Airbag Characteristics

Airbag performance depends on its geometry, venting, and gas supply characteristics as well as on bolster crush force. In the restraint model described here, geometry is specified implicitly by the relations between area, volume, and crush described earlier. The mass of the occupant was fixed (160 lbm) which the gas flow rate (C_o) and duration (t_{off}) and vent size (R_v) were variable. The remaining variables were chosen to represent the characteristics of a realistic restraint system. For example, the time for the restraint system to sense the impact (t_{on}) was chosen to be 10 milliseconds after impact, and it takes about 40 milliseconds before the airbag internal gauge pressure is high enough to cause significant occupant deceleration. These response times are typical of those obtained with current airbag systems.

The gas flow and vent characteristics were chosen in the following way. First, ideal vehicle response was assumed for a 50-mph barrier impact and 42 inches of vehicle crush. Then the gas flow and vent characteristics were varied systematically, and the variations of the five survival criteria in Table 1 were graphed. A temporary set of optimum parameters was then chosen. Finally, selected crash pulses expected in service simulating lower impact speeds (shorter pulse durations) and car-to-car impacts (different shape pulses)* were analyzed.

*See Section IV, Frontal Impact Analysis.

The open parameters in the airbag system were modified so that the system provided adequate response over the range of crash pulses expected. The final set of parameters used in the restraint system analysis is shown in Table 2.

These parameters represent a system that assures survivable performance for the ideally shaped, smooth crash pulse, but does not necessarily minimize the five criteria in Table 1 for any impact. Actual crash pulses are irregular and may result in less than optimum performance of the restraint system. The effect of variations in crash pulse on occupant response is a primary output of the restraint analysis.

Illustrations of this effect are given in Figure 4. Figure 4(a) shows two occupant compartment responses, one the original ideal pulse (solid line) and the second a linearly increasing pulse (dashed line). Both are for 50-mph barrier impacts with 42 inches of vehicle crush. Figure 4(b) plots the acceleration history of the occupant showing the characteristic response obtained with an airbag-bolster system. Note that for the ideal pulse, the peak acceleration is limited by the bolster crush force, but for the triangular pulse the bolster crushes completely and the acceleration shoots up. Figure 4(c) shows the velocity of the occupant relative to the compartment. It is desirable to minimize this parameter even though it is not one of the survival criteria because relative displacement within the compartment will also be minimized. Figure 4(d) shows relative displacement; note that although both final relative displacements are acceptable, the displacement for the triangular pulse is significantly higher than that for the ideal pulse. The CSI, final occupant velocity, and maximum jerk for the two crash pulses are listed in the bottom of the figure. Note the large difference in jerk. Although the final occupant velocities were low in both cases presented here, this parameter is also sensitive to pulse shape and duration.

Table 2

RESTRAINT SYSTEM PARAMETERS

Parameter	Symbol	Value
Mass of occupant	M	160 lbm
Bolster crush force	F_c	7500 lbf
Time for restraint system to sense impact	t_{on}	0.010 sec
End of gas flow to airbag	t_{off}	0.090 sec
Initial clearance between occupant and fully inflated airbag	S_c	0.1 in
Displacement of occupant relative to bolster at which contact area no longer increases	S_f	6.1 in
Displacement of occupant relative to bolster at which airbag volume no longer decreases	S_v	16.1 in
Maximum occupant stroke	D	24.0 in
Maximum occupant/airbag contact area	A_f	320 in^2
Thickness of crushable bolster	B	6 in
Airbag vent gas flow factor	β	0.9
Gas flow into airbag	C_o	16.1 lbm/sec
Ratio of specific heats for the gas		1.4
Initial gauge pressure	P(0)	0.5 psig
Initial gas density	$\rho(0)$	2.8×10^{-4} lbm/in^3
Radius of airbag vent	R_v	1.7 in
Full volume of airbag	V_1	5760 in^3
Minimum volume of airbag	V_2	640 in^3

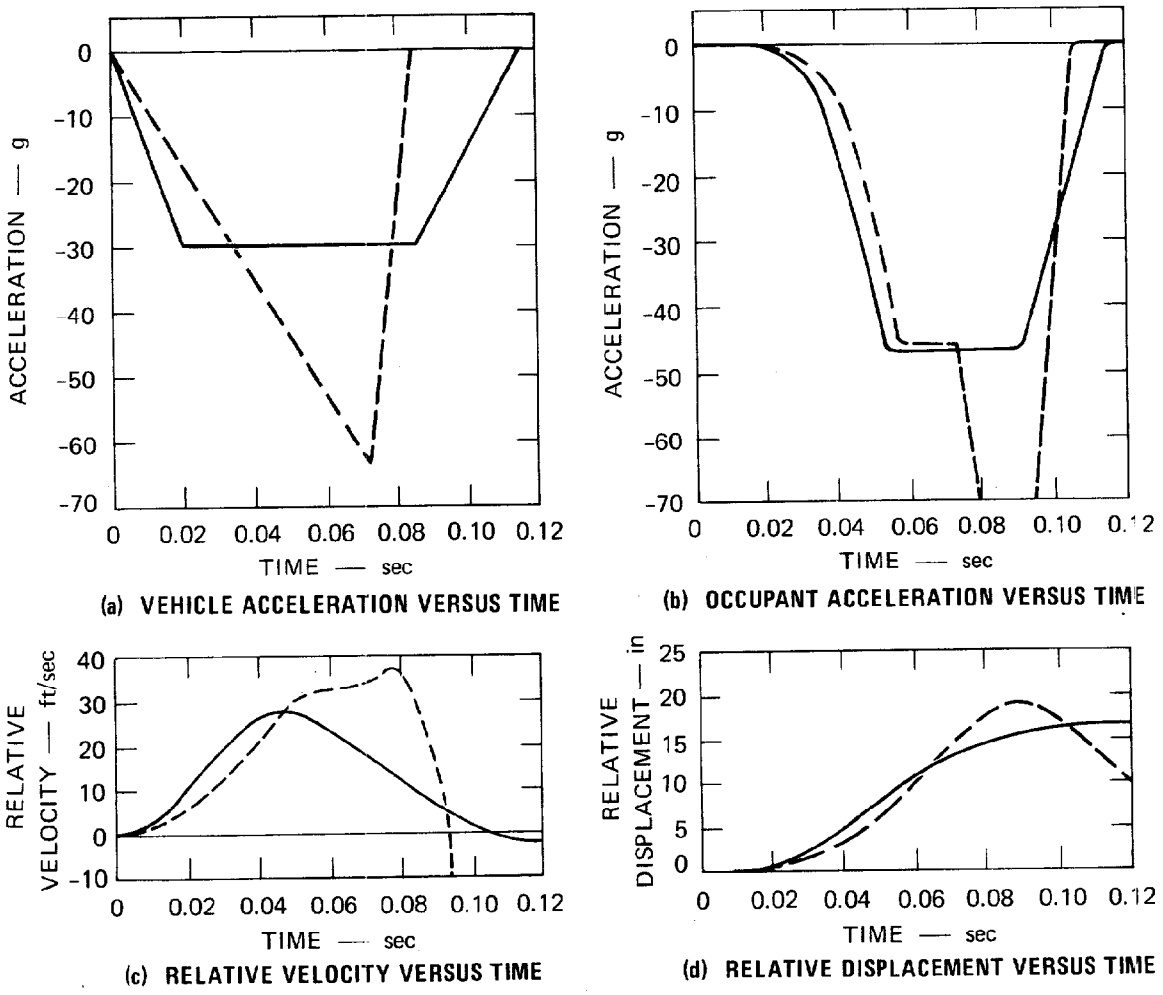

	CSI	FINAL OCCUPANT RELATIVE VELOCITY	MAXIMUM JERK	PEAK OCCUPANT ACCELERATION
Ideal	727	-2.2 ft/sec	2,929 g/sec	46 g
Triangular	3652	-33.0 ft/sec	17,052 g/sec	165 g

MA-3578-14

FIGURE 4 PREDICTED OCCUPANT RESPONSE FOR TWO DIFFERENT OCCUPANT COMPARTMENT ACCELERATION HISTORIES

For each, the impact velocity is 50 mph, the vehicle crush is 42 inches and the rebound velocity is 10 mph.

Although the airbag/bolster restraint system can be made to give acceptable occupant response with very different crash pulse shapes, this comparison shows that vehicle pulse shape does affect response, and may make the occupant pulse unacceptable.

IV FRONTAL IMPACT ANALYSIS

Frontal barrier and car-to-car impacts were analyzed to study the compatibility of three contemporary safety vehicles and to design a subcompact and full-size vehicle system with improved compatibility. The original three safety vehicles were the Minicars subcompact (Reference 6), AMF compact (Reference 5), and the Calspan full size car (Reference 4). The new vehicle system consists of a subcompact design similar to Minicars' and a full size car with the same overall dimensions as the Calspan car. In the analysis used in this study, each vehicle is represented as a system of six masses connected by nonlinear springs as shown in Figure 5. The governing equations for this system are integrated numerically with a computer program (COMPAT), described in Appendix A.

Compatibility of Minicars, AMF, and Calspan Vehicles

The parameters of the three vehicles used in the mass-spring models were developed from available data (References 4-6) and from comparisons of responses predicted by COMPAT and actual crash test results. The mass and stiffness inputs for each vehicle model are tabulated in Appendix B. Longitudinal passenger compartment accelerations measured for the three vehicles in high speed barrier collisions are compared with the accelerations predicted by COMPAT in Figure 6. In each example, the overall response observed in the experiment was predicted by the computer program.

The compatibility of these three vehicles was determined by using COMPAT to simulate 70-mph head-on impacts. Predicted occupant compartment accelerations in the AMF/Calspan head-on collision are shown in

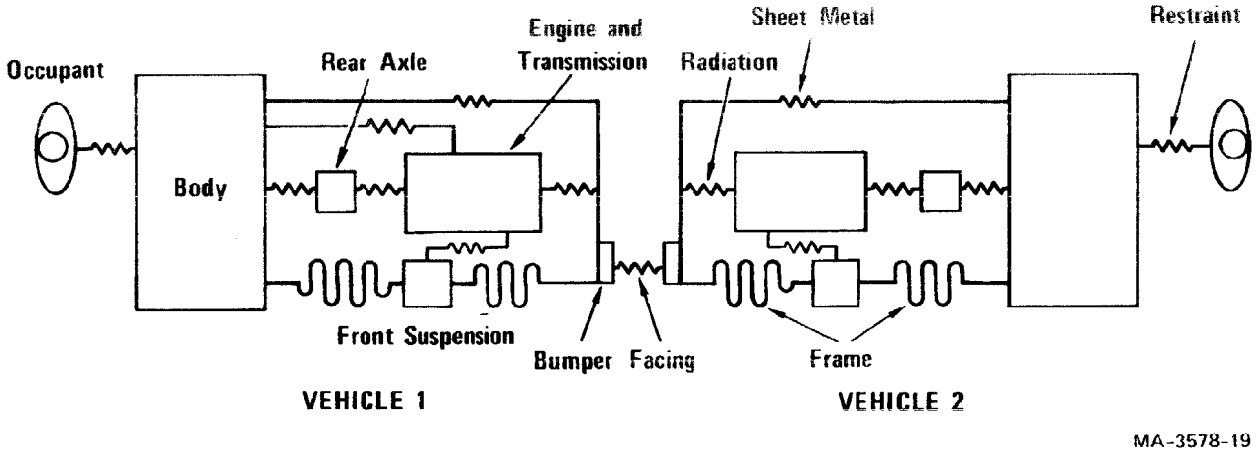

FIGURE 5 IN-LINE IMPACT MODEL REPRESENTING VEHICLES AS A SYSTEM OF MASSES CONNECTED BY NONLINEAR SPRINGS

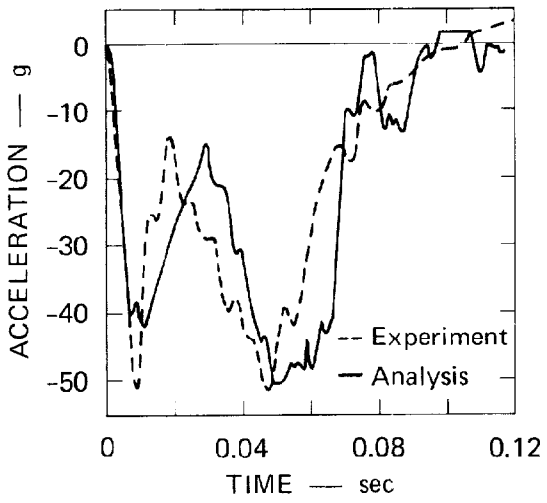

(a) CALSPAN FULL SIZE CAR IN 46-mph BARRIER IMPACT

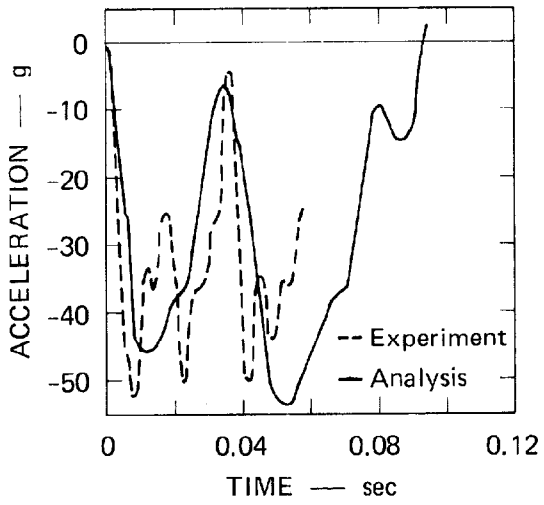

(b) AMF COMPACT CAR IN 50-mph BARRIER IMPACT

MA-3578-20

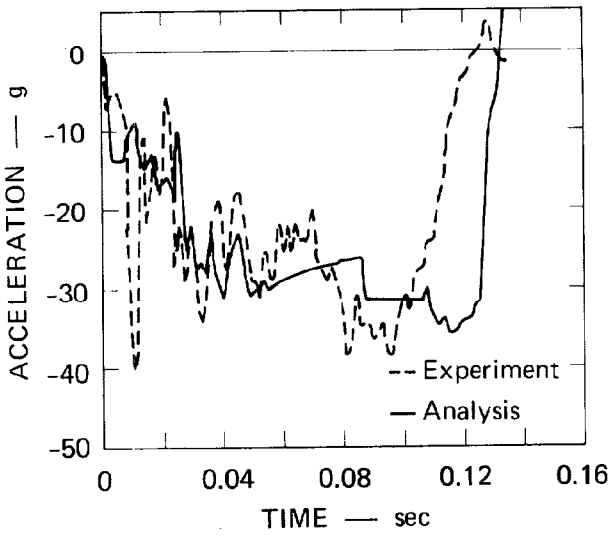

(c) MINICARS SUBCOMPACT CAR IN 50-mph BARRIER IMPACT

MA-3578-21

FIGURE 6 COMPARISON OF MEASURED OCCUPANT COMPARTMENT ACCELERATION WITH COMPAT ANALYSIS

Figure 7. Although the AMF vehicle's acceleration in this collision is only slightly more severe than in its 50-mph barrier collision, the two high acceleration peaks in both collisions make the AMF design unacceptable for occupant survivability. Thus, the AMF car is not compatible with the Calspan car at 70-mph closure speeds. As expected, the Calspan vehicle's acceleration is less severe than in the barrier collision, but the general form of the acceleration curve is altered from that seen in Figure 6(a).

Figure 8 shows the results of the Minicars/Calspan head-on collision. The crash pulse for the Minicars vehicle is not appreciably different from its 50-mph barrier collision, indicating that this design is compatible with the structural characteristics of the Calspan vehicle. Although the peak acceleration of the Calspan car in Figure 8(b) is only 32 g, the pulse is not desirable because its shape is much different from that seen in the Calspan barrier crash. These two vehicles are therefore marginally compatible at 70-mph closure speeds becuase of the tolerant characteristics of the Minicars vehicle. In subsequent tests at 80 mph, however, all the available crush of the subcompact was used and its peak acceleration reached 65 g.

Design of Subcompact/Full-Size Vehicles for Increased Compatibility

The study of the Minicars, AMF, and Calspan vehicles showed that the Minicars vehicle produced nearly the same crash pulse when hitting a barrier at 50 mph as when hitting the Calspan car at 70-mph. This characteristic is desirable because it simplifies restraint system design. The subcompact vehicle has this repeatable crush characteristic because most of the energy is absorbed in the foam filled sheet metal, which crushes at a nearly constant force level. Furthermore, this energy absorbing member crushes independently of the engine, driveline, and frame response. Thus, in the Minicars vehicle, these elements do

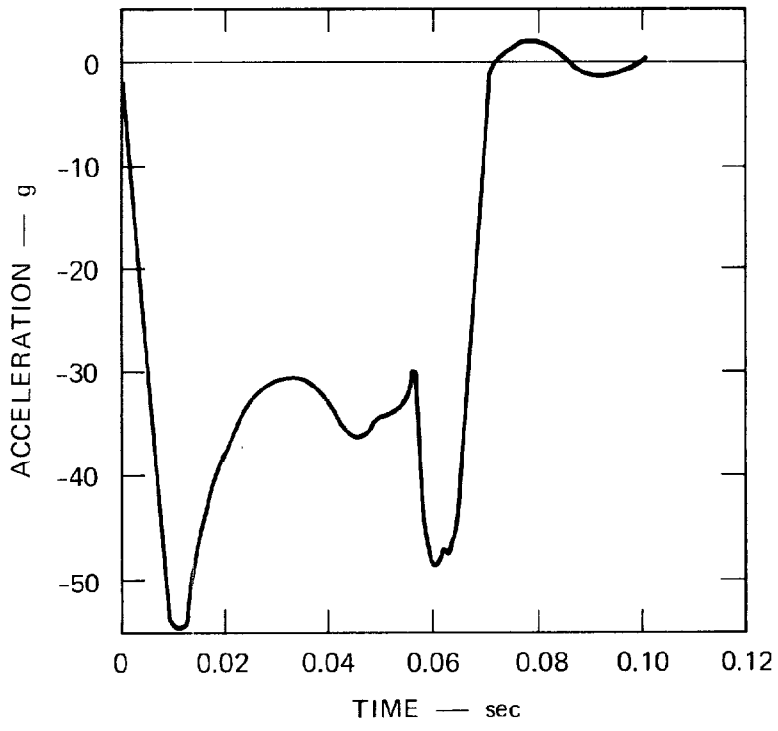

(a) AMF COMPACT CAR

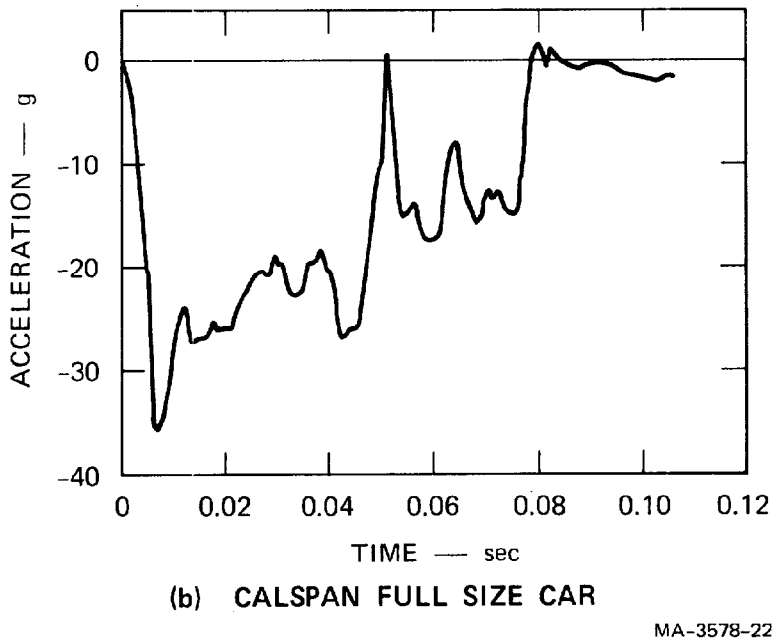

(b) CALSPAN FULL SIZE CAR

MA-3578-22

FIGURE 7 COMPAT SIMULATION OF AMF COMPACT/CALSPAN FULL SIZE CARS IN A HEAD-ON COLLISION AT 70-mph CLOSURE SPEED

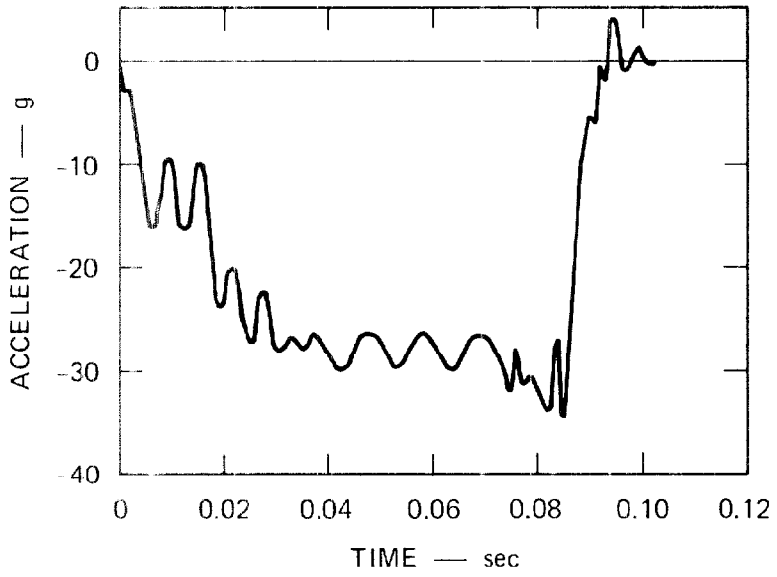

(a) MINICARS SUBCOMPACT CAR

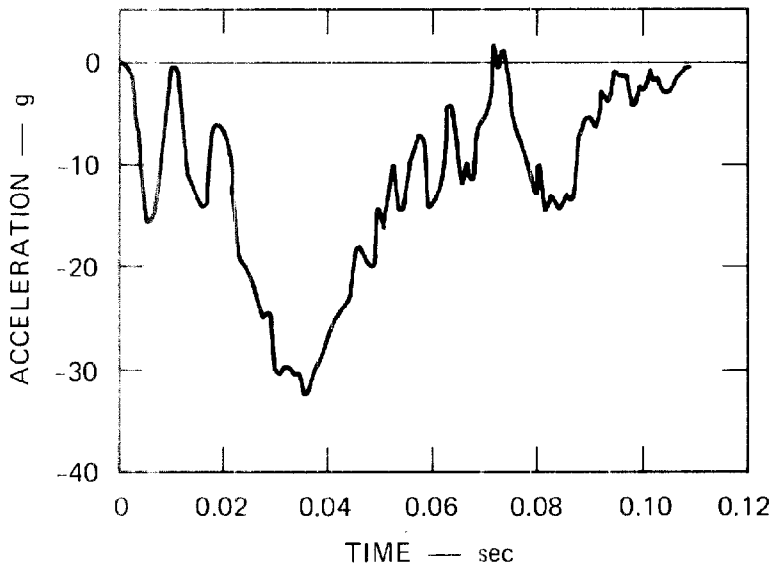

(b) CALSPAN FULL SIZE CAR

MA-3578-23

FIGURE 8 COMPAT SIMULATION OF MINICARS SUBCOMPACT/ CALSPAN FULL SIZE CARS IN HEAD-ON COLLISION AT 70-mph CLOSURE SPEED

not cause any big peaks or valleys in the passenger compartment crash pulse, as are characteristic of the response of the AMF and Calspan vehicles. For these reasons it was decided to design a full-size vehicle using the sheet metal as the principal energy absorbing member. The objectives of the design were to achieve acceptable barrier performance with a smooth crash pulse, and to absorb more energy than the Calspan vehicle in frontal impacts with the subcompact, thus increasing the acceptable closure speed. The force-deflection characteristics of the subcompact vehicle were unchanged, although the structural design was changed as described in the next section. An appreciation for the size limitations on the two vehicles can be gained by examining Figures 9 and 10, which show the layout and principal dimensions of the subcompact and full size cars.

The full size car cannot have a uniform stiffness and corresponding rectangular crash pulse. If a uniform stiffness were used in the large car, its crush force would be higher than the small car's because of barrier impact requirements. Consequently, only the smaller car would crush in a two-car impact. The solution was to give the full size car a two-step force-deflection characteristic; the first step crushes at the force level in the subcompact car, and the second step crushes at a sufficient force to stop the vehicle in a 50-mph barrier impact without excessive crush.

In this two-car system of compatible vehicles, the small car is designed to crush at a nearly constant force F_s determined by its crush stroke and the 50-mph barrier crash requirement. Although the maximum crush stroke in the smaller car (D_s) is 40 inches, its maximum deceleration as in a barrier crash is 30 g (its crash pulse cannot be truly rectangular because of requirements for a low speed no damage bumper). F_s is determined by the body mass M_s and peak acceleration a_s.

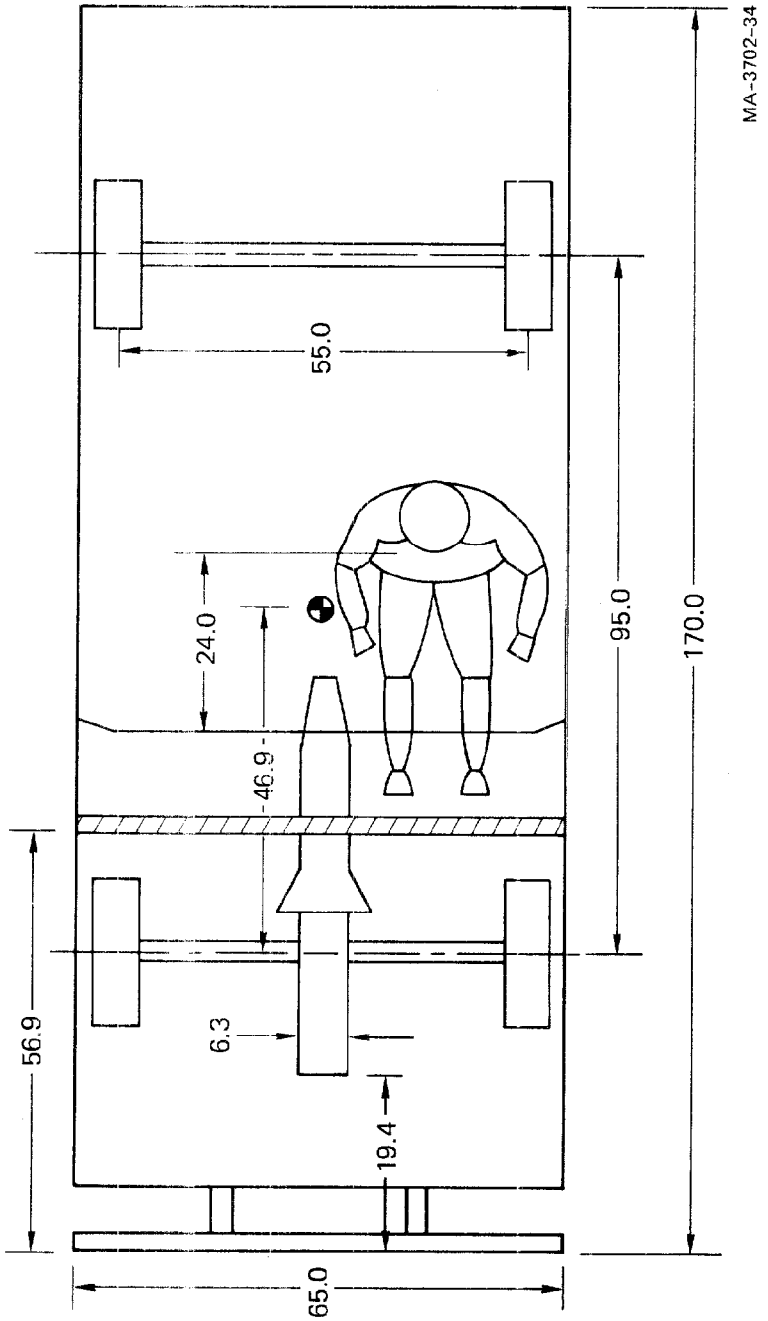

FIGURE 9 LAYOUT DRAWING OF SUBCOMPACT CAR

All dimensions are in inches.

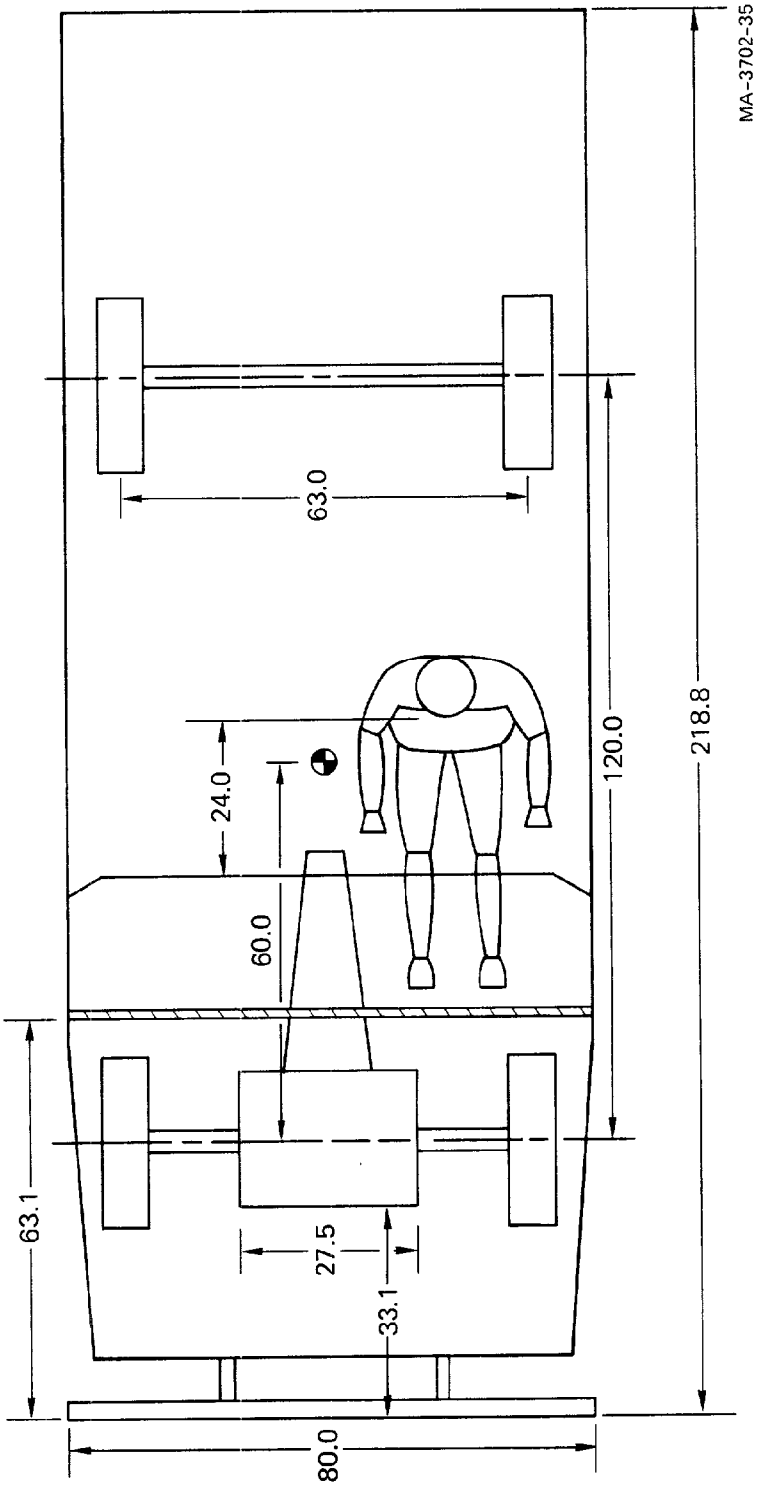

FIGURE 10 LAYOUT DRAWING OF FULL SIZE CAR

All dimensions are in inches.

$$F_s = M_s a_s = 1700 \text{ lbm} \times 30 \text{ g} \tag{19}$$

$$= 51{,}000 \text{ lbf}$$

It is also necessary to specify the maximum acceleration of the large vehicle a_L in a 50-mph barrier crash. In the system described here, a_L is 35 g, which is greater than a_s and, of course, greater than the acceleration the large car would see in a barrier crash if its acceleration could be a constant. Thus, some barrier performance of the large car is sacrificed for increased compatibility with the subcompact car.

The maximum crushing force of the large car is

$$F_L = 3050 \text{ lbm} \times 35 \text{ g} = 107{,}000 \text{ lbf} \tag{20}$$

and its maximum allowable crush (S_L) is 45 inches. Making the softer, forward part of the large car crush at F_s, the length of the soft part of the nose (D_L) can be found by equating the energy absorbed in totally crushing the nose to the kinetic energy of the body at 50 mph (the barrier crash requirement).

$$F_s D_L + F_L (S_L - D_L) = \tfrac{1}{2} M_L V_{50}^2 \tag{21}$$

For the values given here $D_L = 31$ inches. The maximum closure speed V_{mc} in a two-car collision is then found by equating the sum of the energy capacity of the small car and the soft part of the big car to the change is kinetic energy of the two cars in a car-to-car impact.

$$V_{mc} = \sqrt{2 \frac{M_L + M_s}{M_L M_s} F_s (D_s + D_L)} \tag{22}$$

By substitution of the appropriate values into this equation, we obtain $V_{mc} \simeq 90$ mph.

In practice, it is not possible or even desirable to obtain a perfect two-step force-deflection relation for the large car. However, the length D_L was used as a guide, in refining the design of the large car, using the COMPAT computer code. Figure 11 shows the COMPAT predicted response for the large car in a 50-mph barrier impact. Note the double plateau in acceleration. The 47-g peak deceleration at 0.080 sec occurred when the engine hit the firewall after bouncing off the barrier. This effect was not seen in the experiments described later.

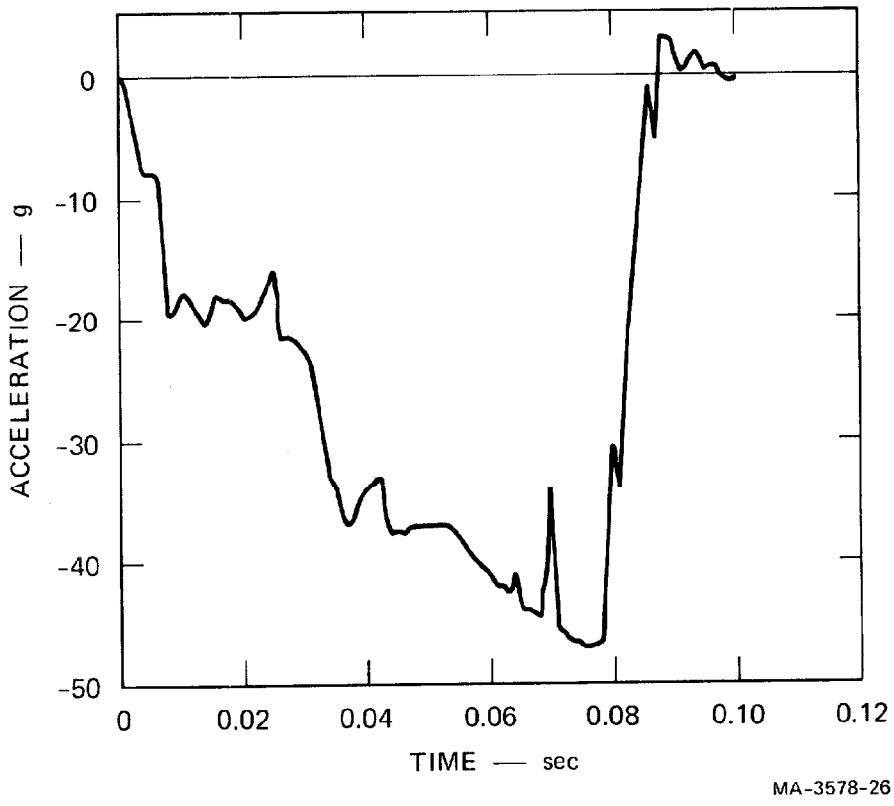

FIGURE 11 COMPAT SIMULATION OF FULL SIZE DESIGN IN 50-mph BARRIER IMPACT

The computer code was then used to predict response in head-on collisions between the subcompact and the new full-size car design. Figure 12 shows predicted body accelerations in an impact at 75-mph closure speed, near the maximum compatible speed. Here the crash pulse in the small car is similar to its barrier impact pulse, while that in the large car has a nearly rectangular shape with an average deceleration of 15 g. The crash pulse in both vehicles is survivable if proper airbag restraint systems are used. Scale model experiments (described in Section V) demonstrated that the crush behavior desired in a vehicle of conventional size and weight, as indicated by the COMPAT program, can be achieved in an actual structure.

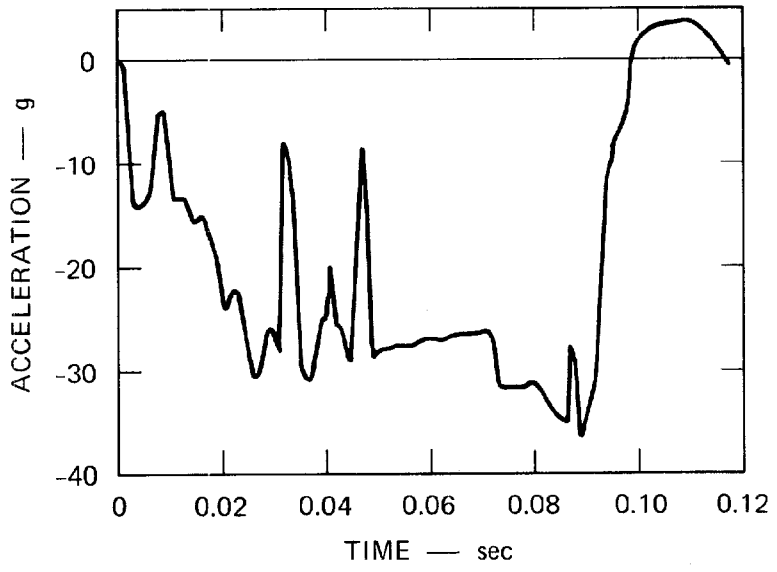

(a) SUBCOMPACT OCCUPANT COMPARTMENT

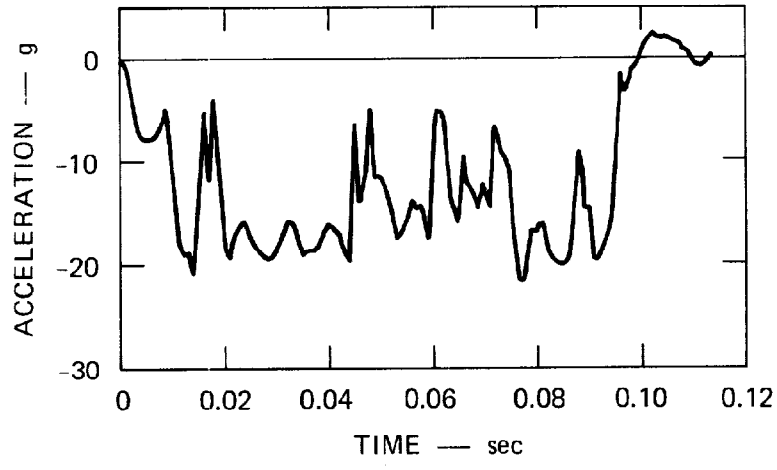

(b) FULL SIZE OCCUPANT COMPARTMENT

MA-3578-27

FIGURE 12 COMPAT SIMULATION OF SUBCOMPACT/FULL SIZE HEAD-ON COLLISION AT 75-mph CLOSURE SPEED

V FRONTAL IMPACT SCALE MODEL EXPERIMENTS

Four experiments were conducted on scale models of the vehicles designed for improved compatibility. Comparison of the first two experiments with corresponding full-scale tests showed that accurate scale models could be made of foam filled sheet metal structures. The second two experiments verified the conclusions of the compatibility analysis described in the previous section. In this process the experimental techniques for the study of oblique impacts were developed.

Scale Modeling Foam Filled Structures

The principal energy absorbing element in the vehicle designs developed in this project is the foam filled aluminum shell. In the scale modeling technique used here the same materials were used in the model as in the prototype, and all dimensions were scaled to one-fifth of full size. The scaled 3003 H 14 aluminum shell was 0.006-inch thick. In the Minicars subcompact vehicle the shell was pop-rivited together and then filled with foam from a foam gun, but these techniques were not feasible with the 1/5-scale models made here. Instead, we spot welded the shells together and poured the foam (before the foaming action occurred) into the shell. It was found that the density and strength of the hardened foam varied significantly with its temperature and with the temperature of the aluminum shell during the pouring process. Furthermore, the pressure of the expanding foam often broke the shell. These difficulties were overcome by burying the foam shell in a sand mold heated to $55^{o}C$. The mold prevented shell breakage and controlled foam temperature. Foam made in this manner had a density of 2.79 lbm/ft^3 and a stress-strain curve approximated by the function:

$$\sigma = 35 \text{ lbf/in}^2 \quad \text{when} \quad 0 \ll \epsilon \leq 0.4$$

$$\sigma = 35 + 390(\epsilon - 0.4)^2 \text{ lbf/in}^2 \quad \text{when} \quad 0.4 < \epsilon \leq 0.75 \tag{23}$$

where σ is compressive stress and ϵ is engineering strain.

Foam material made by casting was used in all the experiments except the scale model duplication of the Minicars full-scale E1 test. In that test, foam samples supplied by Minicars and made with its foam gun were cut to fill the model. These samples had a density of 1.87 lbm/ft^3 and an average strength of 18 psi.

Cart Test

A 34-mph barrier impact test was performed first to determine the dynamic crush characteristic of a scale model foam filled aluminum structure. The test structure is shown in Figure 13(a) before testing and in Figure 13(b) after testing. The rigid cart in this test weighed 9.4 lbm.

The corresponding full-scale crush force for this test structure, determined by multiplying the scaled up acceleration of the cart by the cart's scaled up mass, is plotted as a function of deflection in Figure 14. Also shown is an estimate of the force-deflection curve of Minicars' front ends, estimated by Minicars from static tests. The curve derived from the scaled experiment rises more steeply than the full-scale curve, but both level off at approximately 32,000 lbf. In this example, the crushing of the scale model was not complete and the experimental curve drops to zero at 24 inches.

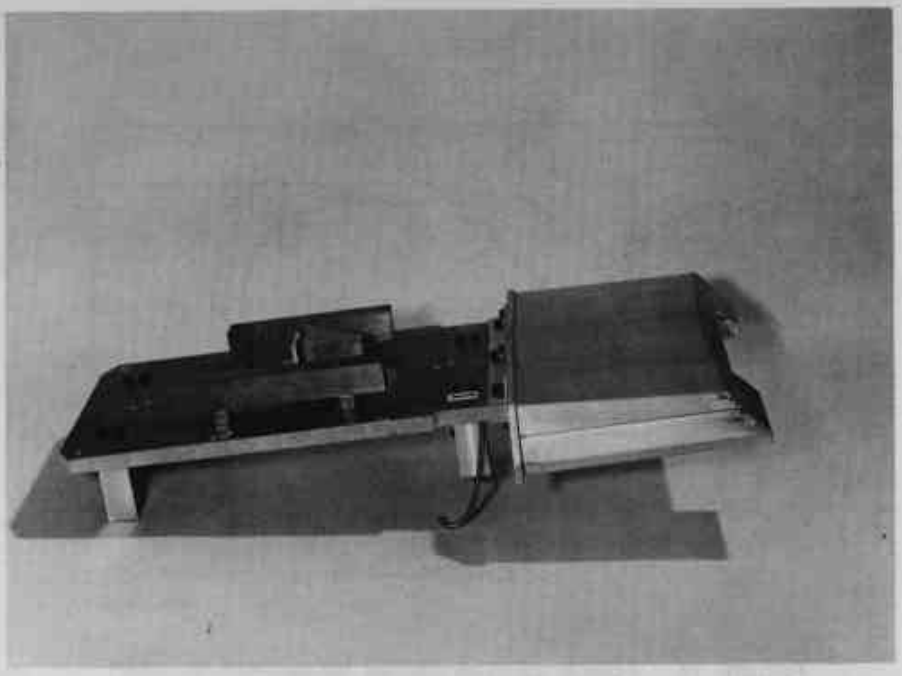

(a) BEFORE IMPACT

(b) AFTER 34-mph BARRIER IMPACT

MP-3702-30

FIGURE 13 1/5-SCALE MODEL OF MINICARS URETHANE FOAM ENERGY ABSORBING NOSE

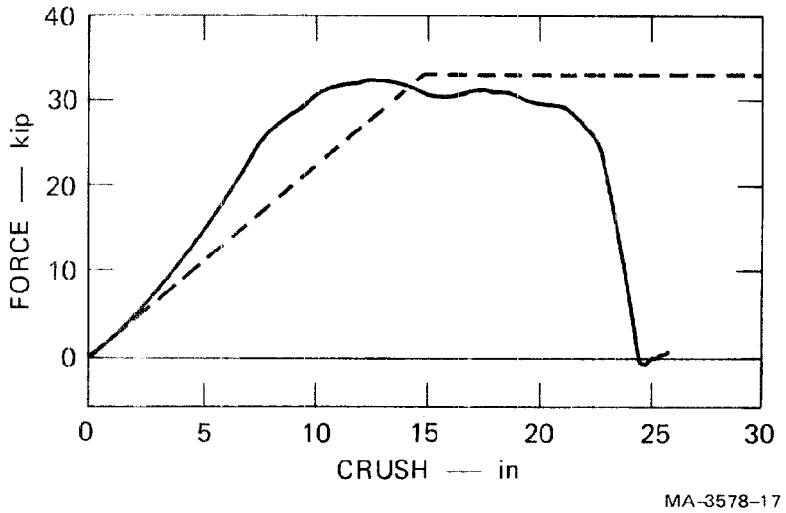

FIGURE 14 FORCE VERSUS CRUSH MEASURED IN CART TEST (——) AND ESTIMATED BY MINICARS (– –)

Minicars E1 Test

A 1/5-scale model was tested in a duplication of a 50-mph barrier test of a Minicars subcompact design, designated the E1 test. The model, shown in Figure 15(a), duplicated in scale the front structure of the Minicars vehicle including engine, firewall, and transmission tunnel, but used a simplified rear structure. Instrumentation in both tests included high speed cameras and accelerometers.

Figure 15(b) shows the 1/5-scale model vehicle after the 50-mph barrier impact test. Examination of the damage after the scale model test and the high speed movies taken during the test revealed that the response was similar to that seen by Minicars in its full-scale test. In particular, the scaled dynamic crush measured in the model was 40 inches compared with 43 inches in the full-scale test.

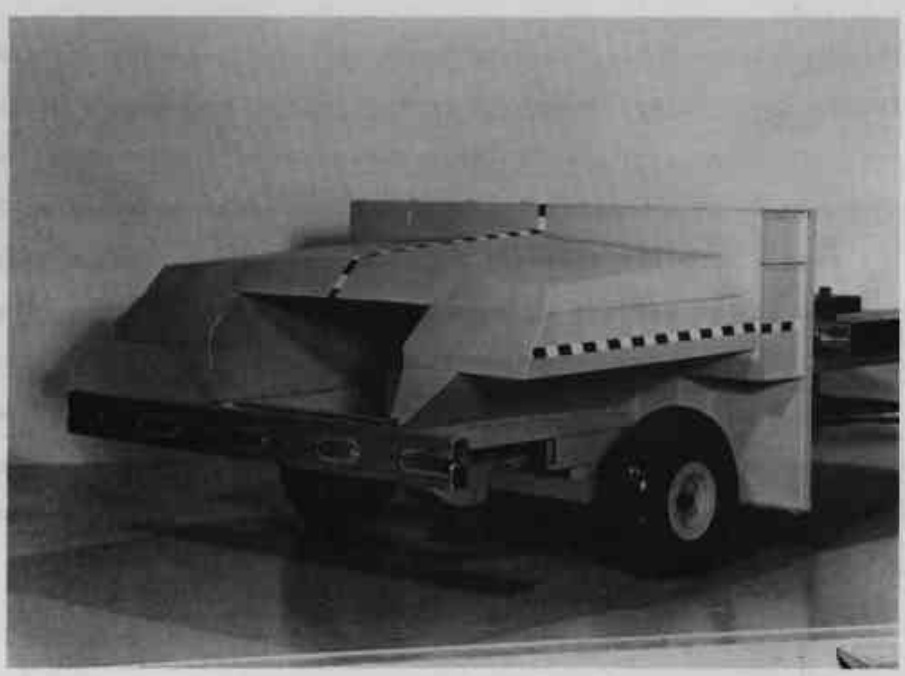

(a) BEFORE IMPACT

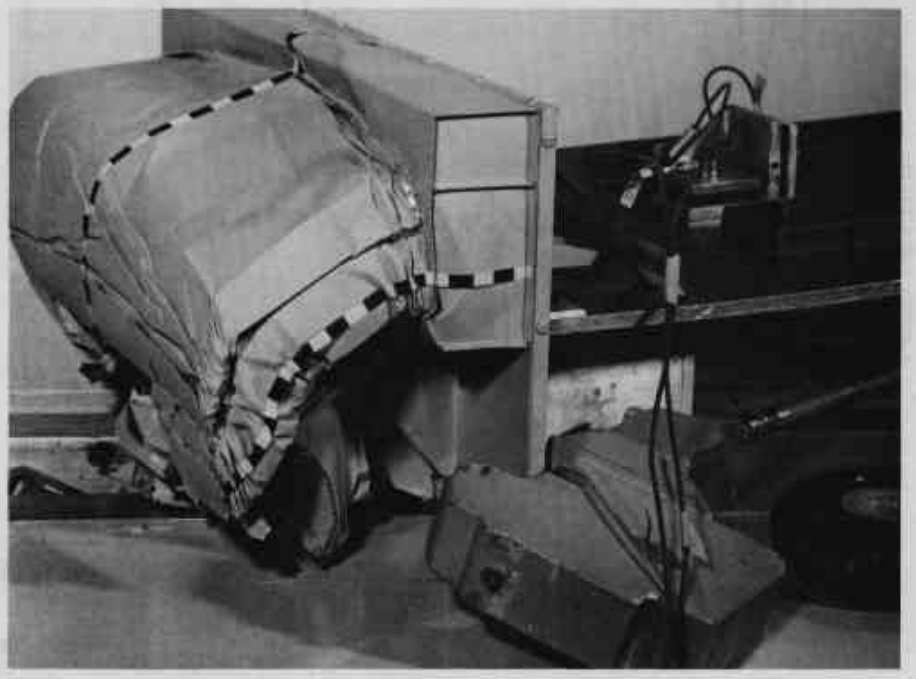

(b) AFTER 50-mph BARRIER IMPACT

MP-3702-31

FIGURE 15 1/5-SCALE MODEL OF MINICARS E1 VEHICLE

The high speed movies in both tests showed a tendency for the nose to climb up the barrier, resulting in the drooped appearance of the crush vehicle shown in Figure 15(b). This observation is supported by a comparison of the accelerometer records from both experiments, Figure 16. The record from the Minicars test was taken by an accelerometer on the trunk of the car and is considered most representative of overall body deceleration. Accelerometers at other points in the body gave records with a different detailed appearance but with the same overall shape and predominant 30-g deceleration level. Because the body of the scaled car is rigid, the model deceleration is representative of the actual body deceleration.

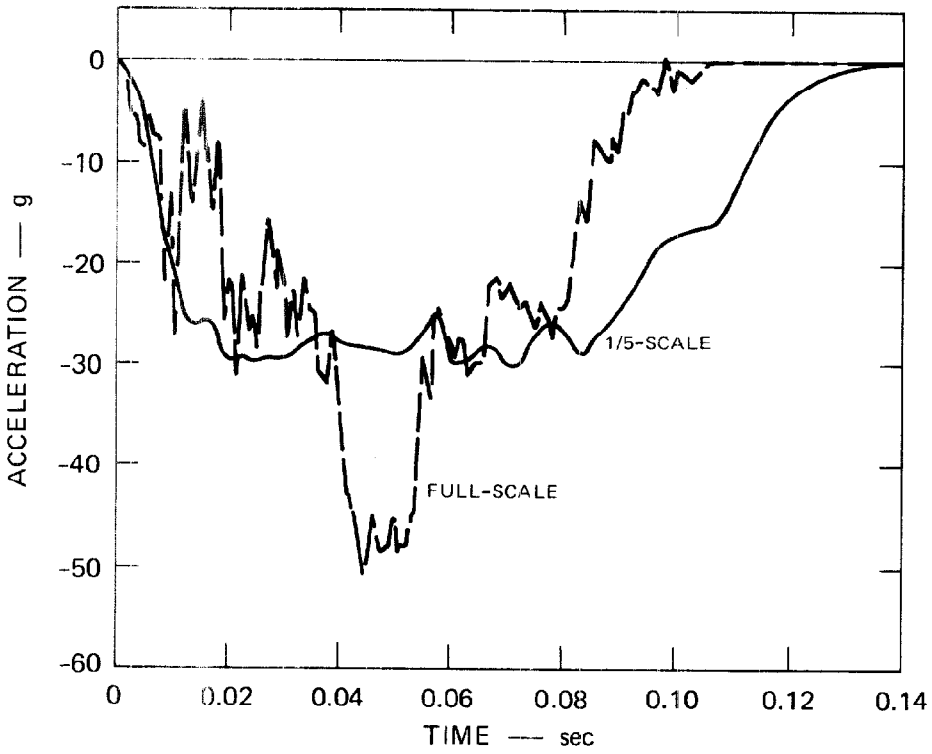

FIGURE 16 COMPARISON OF MEASURED ACCELERATIONS FROM MINICARS E1 TEST (— —) AND 1/5-SCALE TEST (——)

The data from the 1/5-scale test are scaled up for comparison.

The major differences between the two curves are the drop in acceleration between 0.01 and 0.02 sec in the full-scale test and the rise in acceleration between 0.04 and 0.06 sec in the full-scale test. The reason for the first dip is not known and it is not apparent in any other accelerometer records in the test. The hump in the middle of the curve is attributed to the engine's hitting the firewall; this did not occur in the model test or in subsequent tests at Minicars. Thus, both vehicles have a generally uniform acceleration pulse.

This test and the cart test described above showed that scale models could successfully reproduce the behavior of full-scale foam filled shell structures. Although an exact definition of the accuracy of the scaled experiments has not been given, it appears the model tests are as accurate and as reproducible as full-scale tests. This problem will be addressed more fully in the final report.

Subcompact/Full Size Compatibility Experiments

The purpose of the two experiments described here was to demonstrate experimentally the design concepts developed in the frontal impact analysis of subcompact/full size cars. Because the subcompact design was very similar to that used in the E1 test, it was not necessary to run another barrier test with a subcompact. The two tests described here are a 50-mph barrier impact of the full size design and a 77-mph car-to-car impact of the full size and subcompact designs.

The subcompact was modified slightly by the addition of foam elements on the front corners as shown in Figure 17. A 1/5-scale model of the full size design is shown in Figure 18. In this design urethane foam is contained in the thick hood and the vertical pillars that surround the engine. The hood and pillars have a distinct change in cross section midway between the front bumper and firewall, causing a change in crush strength at this point.

FIGURE 17 1/5-SCALE MODEL OF SUBCOMPACT CAR WITH URETHANE ENERGY ABSORBING FOAM NOSE

This design is based on Minicars subcompact vehicle.

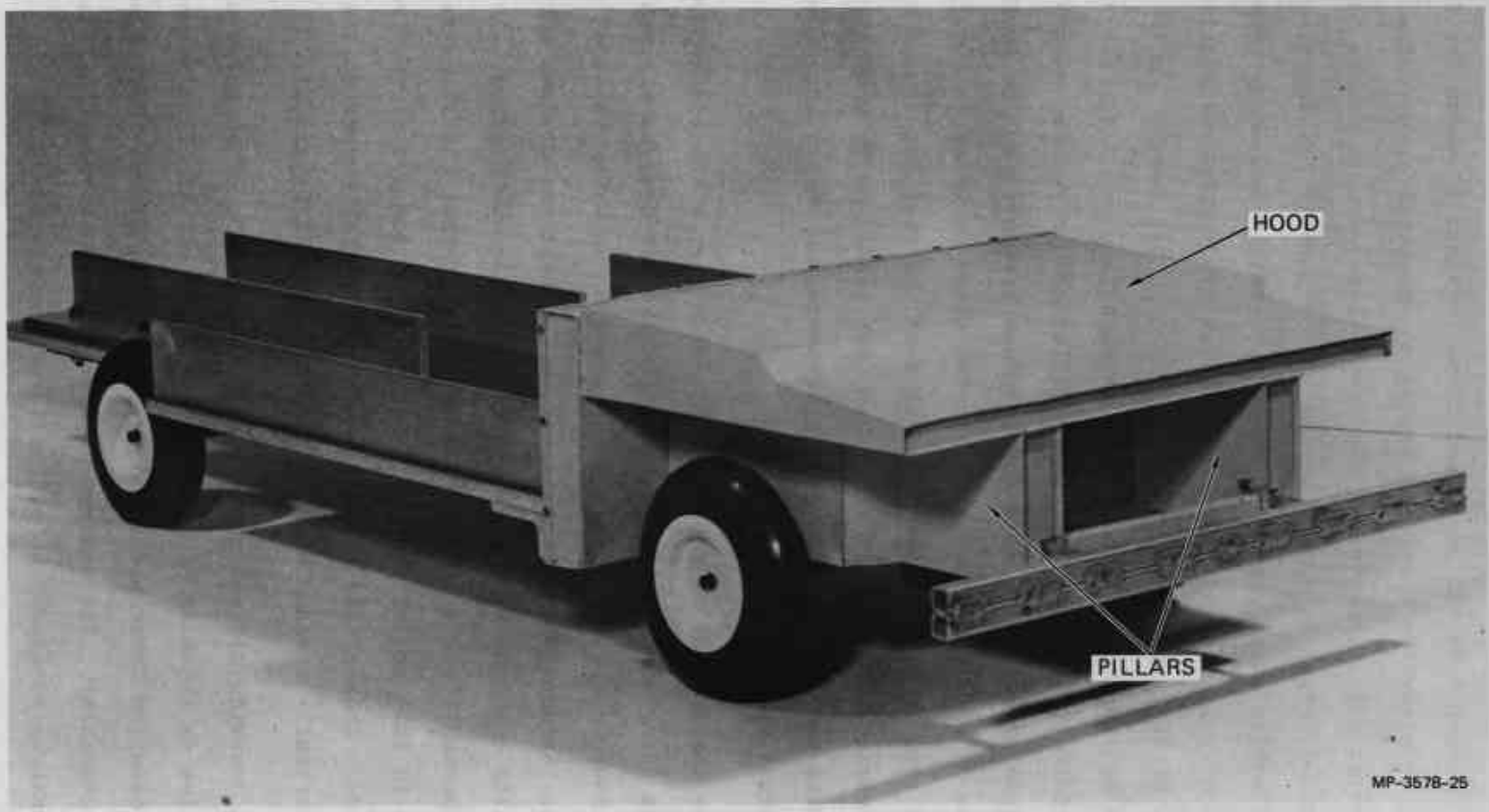

FIGURE 18 1/5-SCALE MODEL OF FULL SIZE CAR WITH URETHANE FOAM ENERGY ABSORBING NOSE

The barrier test was performed first. Figure 19 shows the full size vehicle after the test, and Figure 20 shows the longitudinal accelerometer data taken during the test. The curve in Figure 20(c) (acceleration versus crush) shows that the structure has the two-step force-deflection curve desired. However, a slight dip occurred near 30 inches of scaled crush. This dip was attributed to the buckling of the hood, evident in Figure 20. This buckling was avoided in later experiments by improving the fastening between the hood and pillars, but it does indicate that long thin foam filled structures can be unstable. A comparison of Figure 20 with the response predicted by the COMPAT simulation (Figure 11) shows that the two steps occur at the correct level and time in the barrier test but that the peak acceleration seen in the experiment (36 g) was less than that predicted by COMPAT (47 g). As mentioned earlier, this is due to the more controlled engine response in the actual test.

After the barrier test of the full-size car, a two-car head-on experiment using the subcompact and full-size car designs was run at a 77-mph closure speed. The two vehicles are shown after the test in Figure 21. As desired, the small car in the test was crushed to its limit, while only the soft part of the large car was crushed. At impact, the small car was about 5/8 inch higher than the large car (3 inches in full scale) eventually causing the bumpers of the two cars to override. This is the reason for the protruding bumper of the large car and partially crushed hood of the small car in Figure 21.

This override did not significantly affect the crash pulse of the two vehicles as shown in Figure 22. Again the actual crash pulses closely resembled those predicted by COMPAT (see Figure 12) and were nearly rectangular. The maximum acceleration of the small car was 30 g and the maximum acceleration of the large car was 22 g.

FIGURE 19 1/5-SCALE MODEL FULL SIZE VEHICLE AFTER 50-mph BARRIER IMPACT

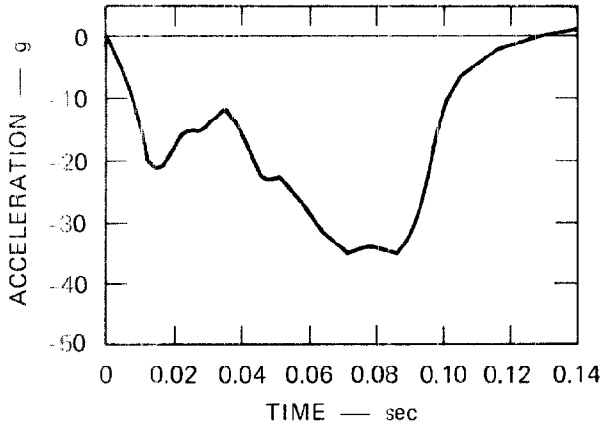

(a) ACCELERATION VERSUS TIME

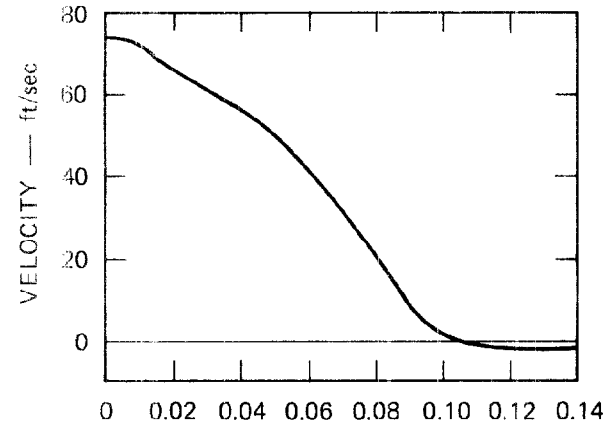

(b) VELOCITY VERSUS TIME

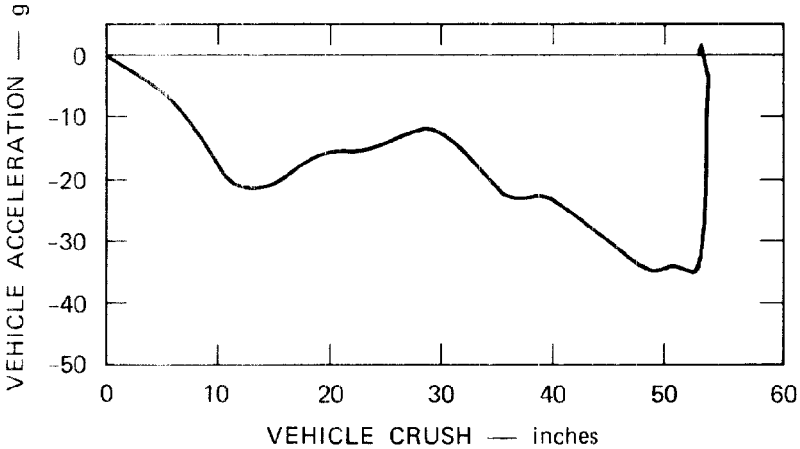

(c) ACCELERATION VERSUS CRUSH DISTANCE

MA-3578-28

FIGURE 20 LONGITUDINAL ACCELERATION OF FULL SIZE VEHICLE IN 50-mph BARRIER IMPACT

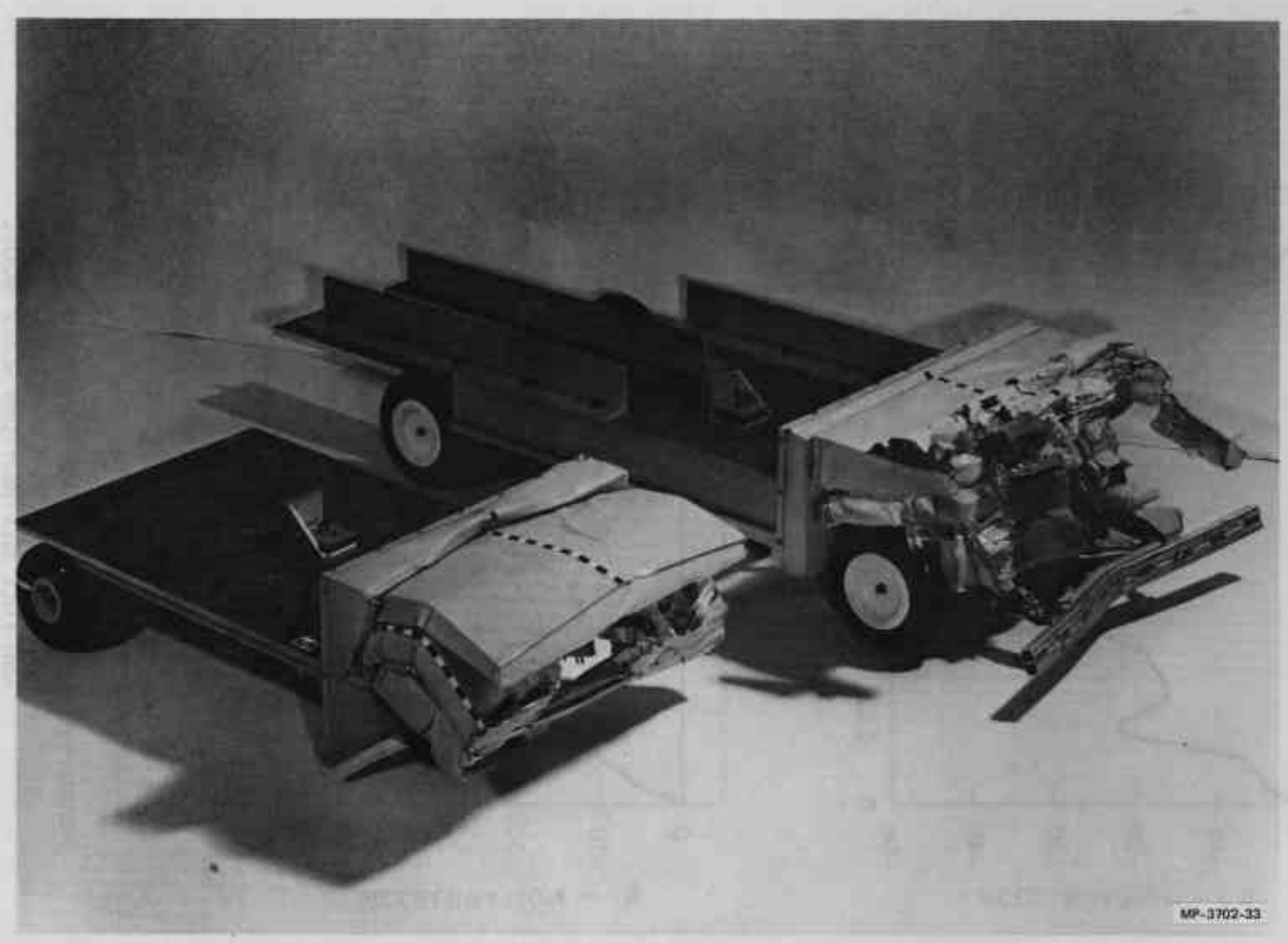

FIGURE 21 1/5-SCALE MODEL SUBCOMPACT AND FULL SIZE VEHICLES AFTER 77-mph HEAD-ON COLLISION

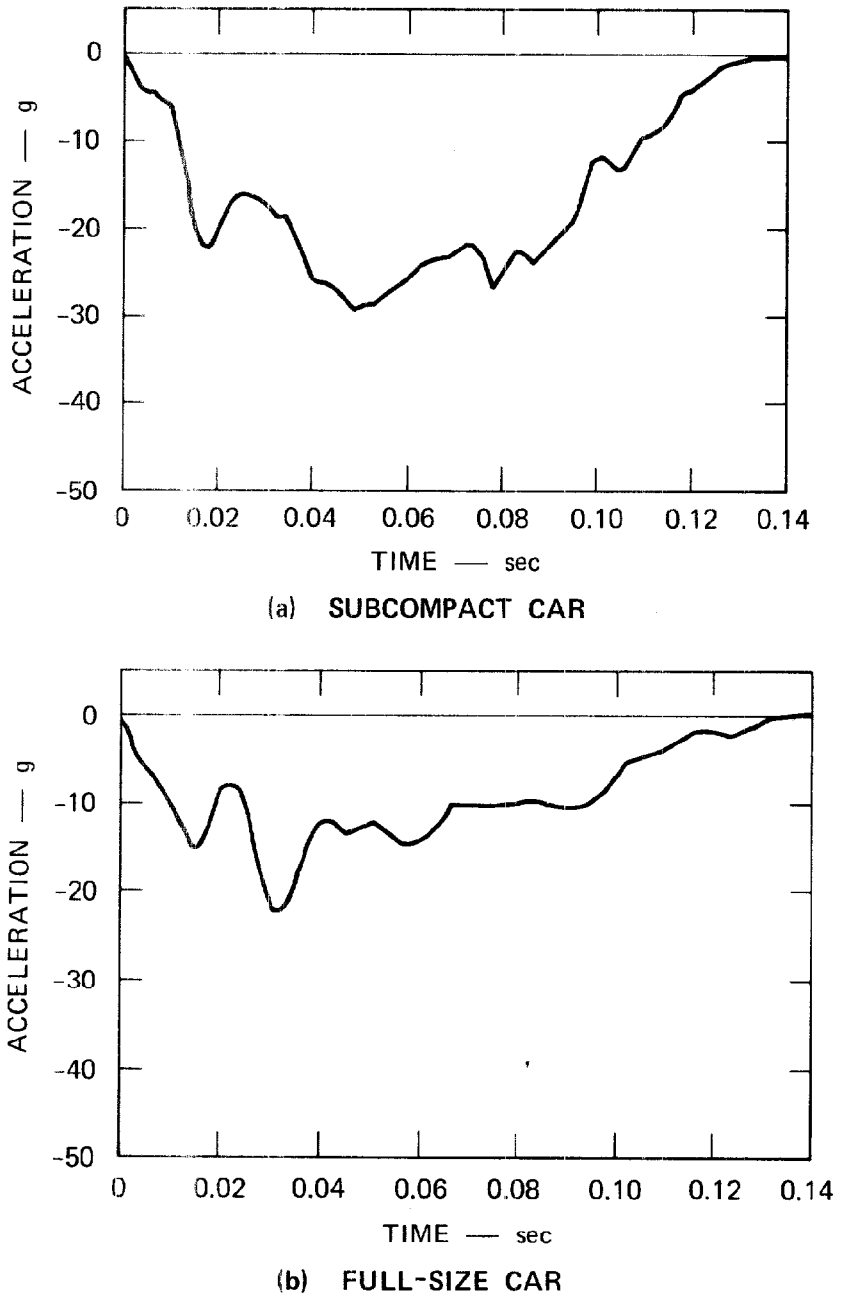

FIGURE 22 LONGITUDINAL PASSENGER COMPARTMENT ACCELERATIONS FOR SUBCOMPACT (TOP) AND FULL SIZE (BOTTOM) SCALE MODEL VEHICLES IN 77-mph FRONTAL IMPACT TEST

When the crash pulse from each vehicle was analyzed with the restraint model, it was found that occupants in both cars could survive. In the larger car the restraint model predicted a CSI of 170, a jerk of 1733 g/sec, an occupant translation of 8.9 inches, and a residual velocity of 3.5 ft/sec. In the small car the corresponding values were: 540 CSI, 2397 g/sec jerk, 12.8 inches translation, -1.0 ft/sec residual velocity.

These two experiments demonstrated that compatibility between subcompact and full-size cars can be achieved in head-on impacts at 75 to 80 mph. They also demonstrated the accuracy of scale modeling foam filled structures.

VI MODELING AUTOMOTIVE SHEET METAL STRUCTURES

The purpose of this investigation is to extend the scale modeling of automobile structures to include sheet metal components and to find the cost and fidelity of scaled sheet metal structures in crashworthiness experiments. For this purpose, we compared the full-scale 20-mph barrier impact test* of the front end sheet metal of a 1968 Plymouth Fury with a corresponding 1/5-scale model test. The purpose of the full-scale test was to determine the energy absorbed by the sheet metal. Consequently, the frame and driveline were removed from the Plymouth. This made the comparison with the scaled experiment a strict test of model accuracy, because no structure other than the sheet metal could influence vehicle response.

Model Fabrication

A complete 1968 Plymouth Fury front end was used as a guide in construction of the scale model, providing dimensions, construction details, and tensile coupons for testing. The principal components of the front end sheet metal are the fenders, inner wheel wells, hood, and radiator support. Since all these parts except the radiator support have compound curves, brake formed parts with simple curves will not accurately model their response. Therefore, an explosive forming technique was used to fabricate most of the sheet metal parts for the 1/5-scale model.

*Dynamic Science Test 289-49, Reference 3.

Five of the large contoured parts of the model, the two fenders, the inner wheel wells, the hood, and the hood brace, were formed at SRI using explosives. The forming technique used consists of four steps:

(1) Production of 1/5-scale patterns

(2) Hand forming a male wooden punch from the patterns

(3) Casting of an aluminum die from the punch

(4) Explosive forming of sheet metal with the die.

In the first step, 1/5-scale patterns of cross sections spaced regularly at 2-1/2 inches are drawn directly from full-scale parts using a pantograph. Then, half-inch-thick balsa sections are cut out from these patterns and laminated to produce a roughly contoured form. The rough form is then filled and sanded to fashion a smoothly contoured male punch. In the third step, a solid aluminum female die is pressure cast from each male wooden punch, and the top surface of the die (surrounding the cavity) is milled flat to allow a good seal between the die and the sheet metal blank during the actual forming of the parts.

In the last step of the explosive forming process, a sheet metal blank is clamped between the die and a 3/4-inch aluminum draw ring, and the die cavity is evacuated through a 1/8-inch-diameter evacuation hole drilled into the cavity through one side of the die. An explosive charge is positioned over the metal blank, the entire assembly is placed in a tank of water as shown in Figure 23, and the charge is detonated. The proper charge amount, charge shape, and standoff distance are found for each different part by trial and error. Figure 24 shows the wooden male punch, the aluminum die, and the as-formed sheet metal for a fender of the scale model. After forming, the explosively formed parts are trimmed of excess flashing; reverse bends, which could not be formed explosively with a single die, are hand formed.

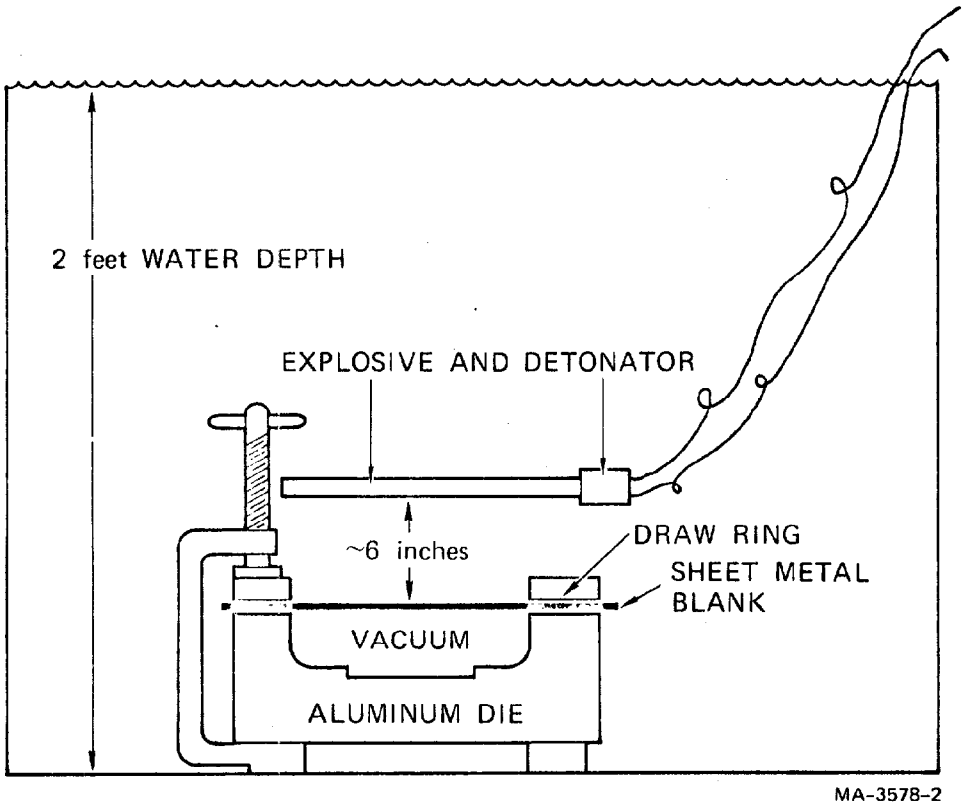

FIGURE 23 EXPLOSIVE FORMING SETUP

Figure 25 compares the finished 1/5-scale model sheet metal structure with the full-scale sheet metal structure. In the model the outer fenders, wheel wells, hood, and hood brace were all explosively formed. All the other parts such as the radiator mounting, the grill, and various braces and brackets were brake formed. Joints used in assembly (spot welds, solder joints, and bolts) were matched as closely as possible to the full-scale structure. Figures 26 and 27 provide additional visual comparison of the 1/5-scale model with the full-scale automotive sheet metal.

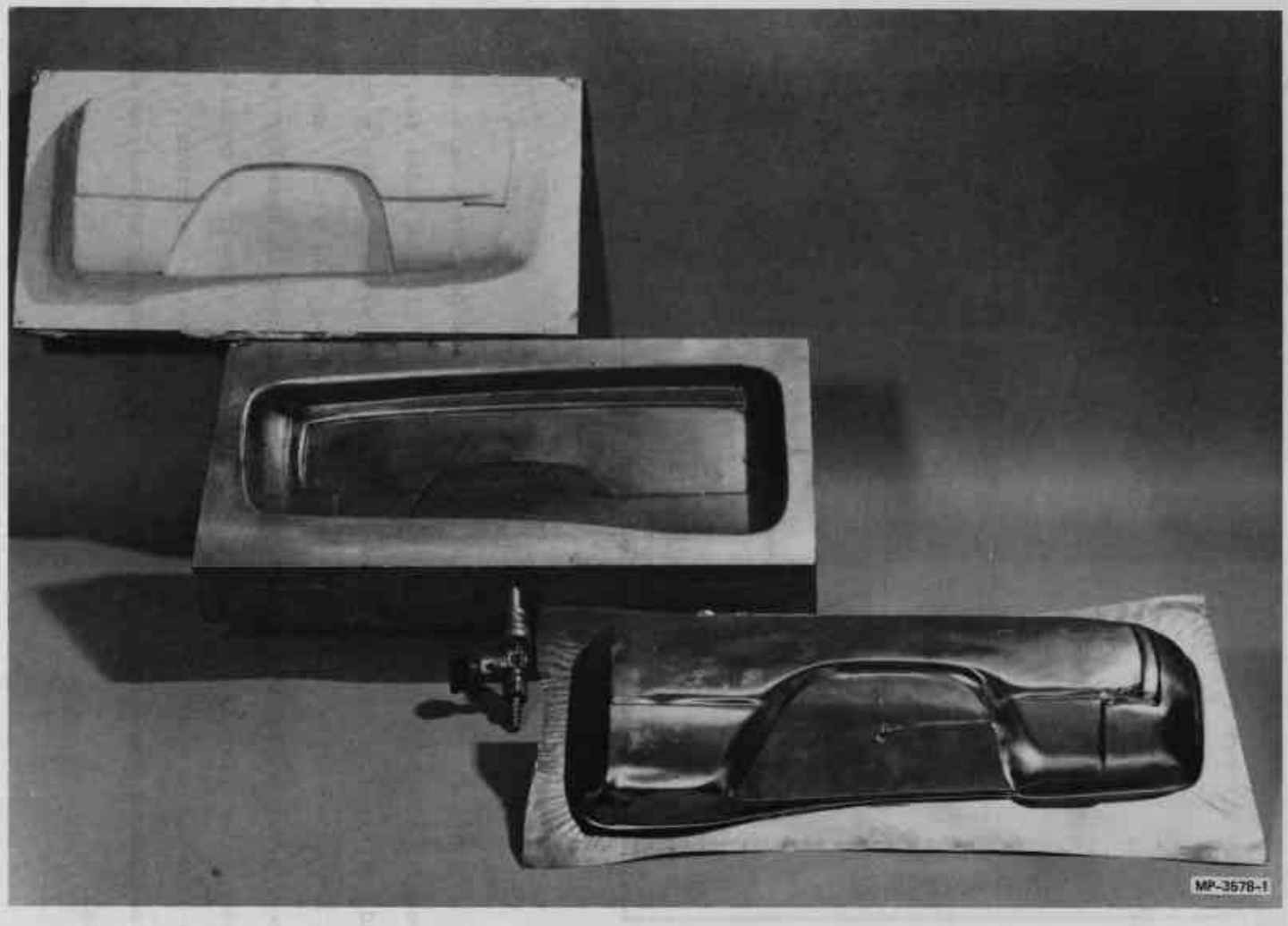

FIGURE 24 THREE STEPS IN EXPLOSIVE FORMING OF SHEET METAL PARTS
Wooden Male Bunch (Top), Aluminum Die (Center) and As-Formed Part (Bottom).

(a) FULL-SCALE

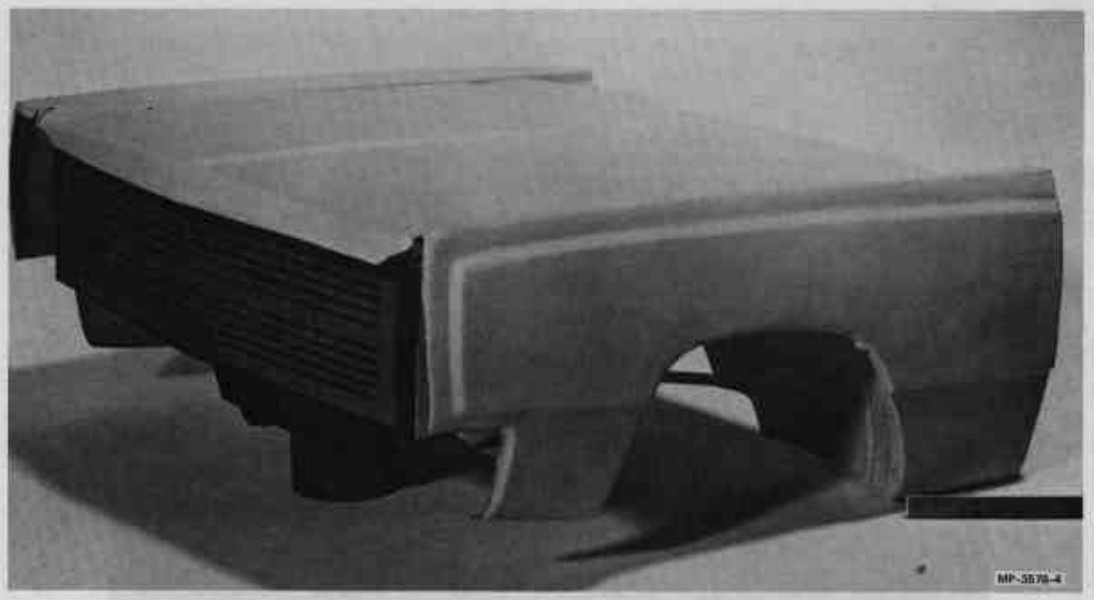

(b) 1/5-SCALE

FIGURE 25 FRONT SHEET METAL ASSEMBLY FULL-SCALE (TOP), 1/5-SCALE (BOTTOM)

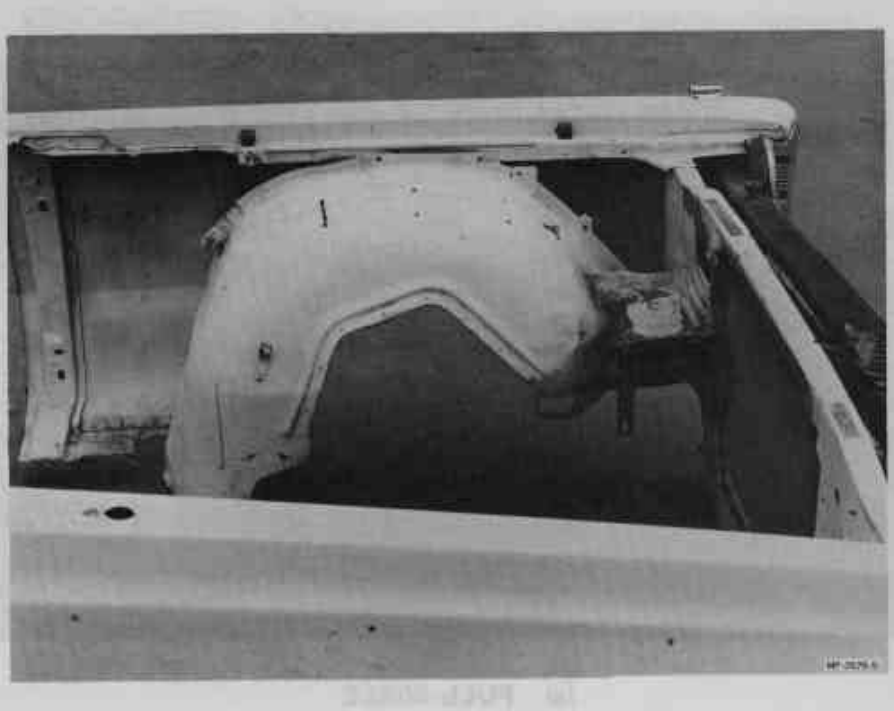

(a) FULL-SCALE

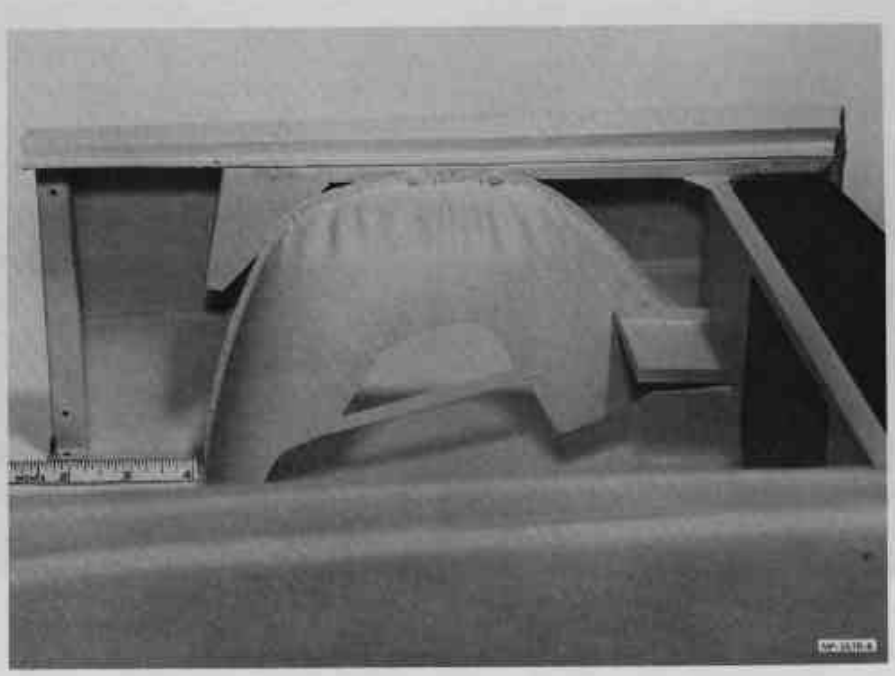

(b) 1/5-SCALE

FIGURE 26 COMPARISON OF FULL-SCALE AND 1/5-SCALE SHEET METAL AS VIEWED FROM SIDE WITH HOOD REMOVED

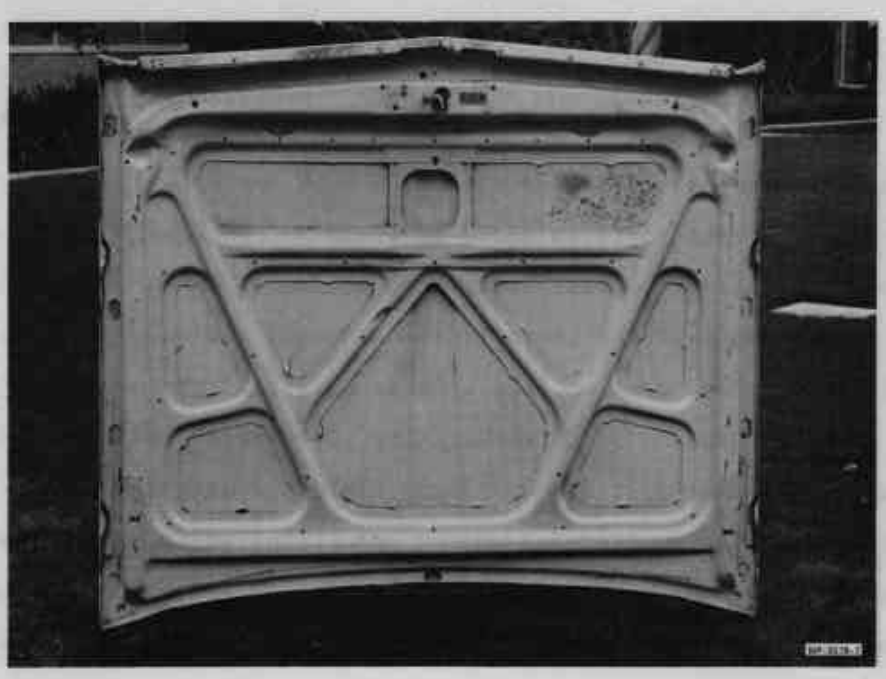

(a) FULL-SCALE

(b) 1/5-SCALE

FIGURE 27 FULL-SCALE AND 1/5-SCALE HOOD UNDERSIDES

The hood brace is attached with soft plastic resin.

Model Fidelity

A more quantitative measure of model fidelity was made by comparing measurements of full-scale parts with corresponding measurements of the scale model parts as shown in Table 3. The percent difference between the full-scale measurement and the model measurement scaled to full size shows that the overall dimensions of the scale model are within 2% of those desired, the average material thickness is 6% greater than desired, and the yield strength is 10% greater than desired. The differences in material thickness and yield strength are caused by stretching of the sheet metal during the explosive forming process. Since the amount of stretching is a function of the thickness and temper of the sheet metal blank, it is difficult to compensate for it completely. Because the crush strength of the sheet metal depends mostly on its resistance to plastic bending, these differences in thickness and yield strength resulted in a stronger model than desired. The added strength of the model is proportional to the difference in thickness (Δt) squared and the difference in yield strength $(\Delta\sigma_y)$, and can therefore be estimated as

$$S + \Delta S = \frac{(t + \Delta t)^2 (\sigma_y + \Delta\sigma_y)}{t^2 \sigma_y} \tag{24}$$

$$S + \Delta S \cong (1.06)^2 (1.10)S = 1.25S$$

or an added strength of 25 percent. As discussed below, the actual difference in strength, as indicated in the 1/5-scale experiment, was less than 25 percent.

The body of the scale model was a system of plates whose mass, center of gravity, and moments of inertia were scaled from those of the full-scale vehicle. These values are tabulated in Table 4 along

Table 3

COMPARISON OF SHEET METAL DIMENSIONS AND STRENGTHS

		Full-Scale	1/5-Scale	% Difference[a]
Overall Dimensions	Width at firewall	78 in	15-1/4 in	- 2.2%
	Fender length	66 in	13-1/4 in	+ 0.4%
Material thickness	Fender thickness (lower side)	0.0355 in	0.0073 in	+ 2.8%
	Fender thickness (top)	0.0347 in	0.0075 in	+ 8.1%
	Tensile specimen thickness (from mid-fender)	0.0348 in	0.0075 in	+ 7.8%
	Average thickness	0.0350 in	0.0074 in	+ 6.2%
Tensile test results	Yield strength	27,300 psi	29,900 psi	+ 10%
	Tensile strength	42,800 psi	48,000 psi	+ 12%
	Percent elongation	41.4%	35.4%	- 14%

[a]Percent difference between full-scale measurement and the model measurement scaled to full size.

with corresponding full-scale values. Figure 28 (a) and (b) shows the completed model being placed on the launcher before testing.

Table 4

COMPARISON OF MASS AND INERTIA PROPERTIES
OF FULL-SCALE AND 1/5-SCALE VEHICLES
IN SHEET METAL TESTS

	Full-Scale	1/5-Scale	% Difference
Sheet metal weight	250 lb[a]	2.27 lb	+13.5%
Body weight	2415 lb[a]	20.53 lb	+ 6.3[a]
Total weight	2665 lb	22.80 lb	+ 6.9
Inertia (pitch) for body center of gravity	3.5×10^6 lbm-in^2	1192.7 lbm-in^2	+ 6.5[a]
Body center of gravity to firewall	68 in[a]	12.91 in	- 5.1[a]
Center of gravity to ground	21 in[a]	4.0 in	- 4.8

[a]Estimate.

Test Comparison

The response of the full-scale and the scale model tests were compared on the basis of high speed movies and accelerometer data taken during the tests and by inspection of the vehicles after the tests. Parts of the high speed movies from the two tests are shown in Figure 29. Pictures taken at corresponding times* in the two experiments show that

*Note that events occur 5 times faster in the scale model experiment so that the picture taken at 50 msec in the full-scale test in Figure 29 corresponds to the picture taken at 10 msec in the 1/5-scale test.

(a)

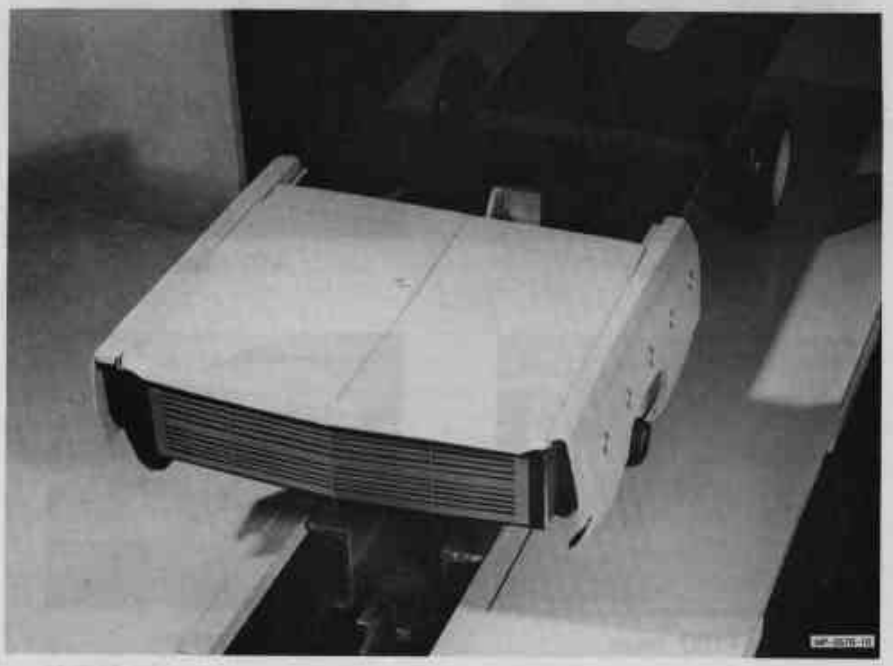

(b)

FIGURE 28 1/5-SCALE MODEL BEING PLACED ON LAUNCHER BEFORE EXPERIMENT

The model weighs 21 pounds.

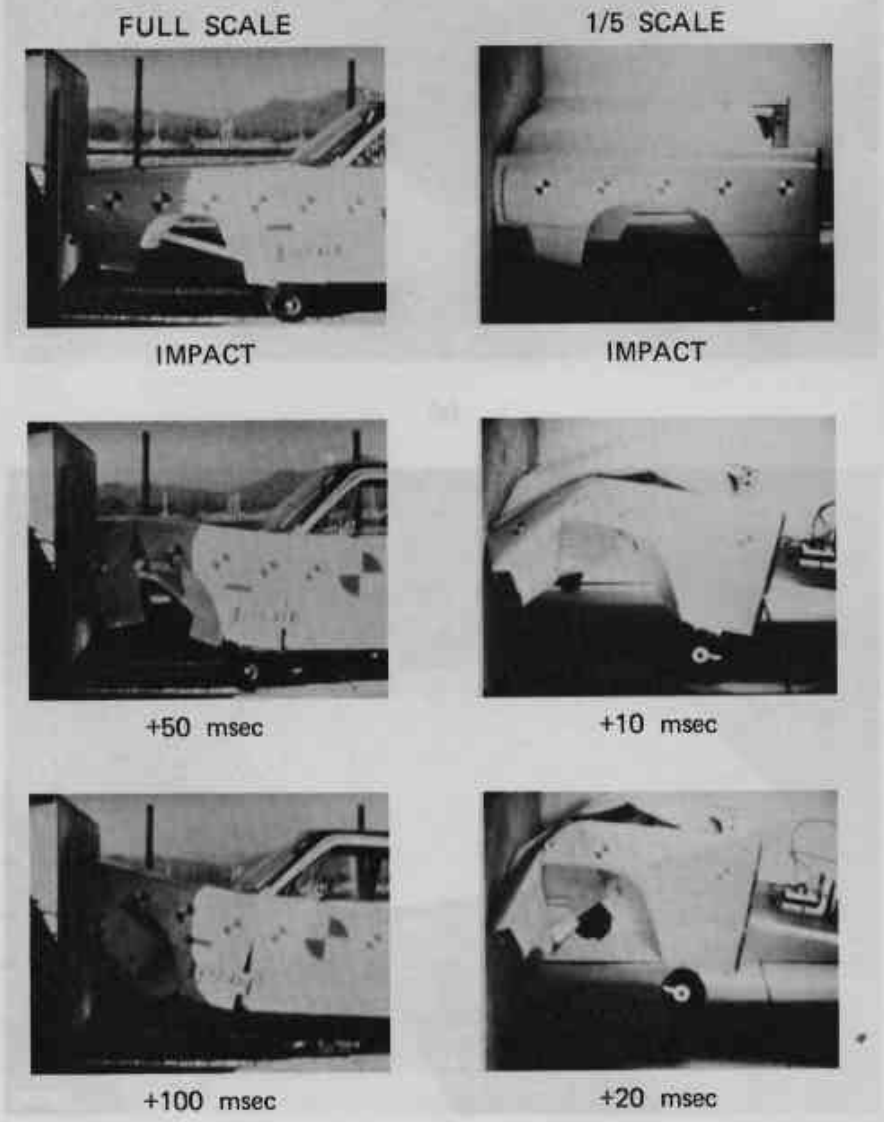

FIGURE 29 COMPARISON OF MOVIES TAKEN DURING SHEET METAL EXPERIMENTS

not all details of the full-scale test were reproduced in the scaled test. In particular, the hood buckled first at the front in the full-scale test, but buckled near its middle in the model test. Also, the final crush was about 33 inches in the full-scale test and 22 inches in the 1/5-scale test.

The difference in hood response was attributed to a possible difference in hood attachment at the front. The scale model hood was rigidly bolted down; the method of full-scale hood attachment is unknown, but if the existing latch had been used, it would probably have broken on impact.

The difference in crush was attributed to the higher than desired yield strength and material thickness in the model. A photograph of the 1/5-scale model after the test is shown in Figure 30. The dynamic crush during the scale model test was greater than the deformation seen in Figure 30; but not as great as that in the full-scale test where the grill rolled completely under and was facing the ground after the test. The increased stiffness of the scale model is also seen in the longitudinal accelerations measured during the tests, shown in Figure 31, scaled to full size for comparison.

The similar shape of the acceleration-time curves in the two tests is evident in Figure 31(a), but the model acceleration lags behind the full-scale acceleration because the increased stiffness in the model slows it more rapidly, as seen in Figure 31(b). Thus corresponding modes of response are reached at different times in the two tests. This effect is partially eliminated by comparing acceleration versus crush,* in Figure 31(c). Here, the similarity of response is more apparent.

A measure of accuracy of the model test can be obtained by comparing the peak accelerations in Figure 31(a), the energy absorption,

---

*Crush was approximated by integrating longitudinal acceleration twice.

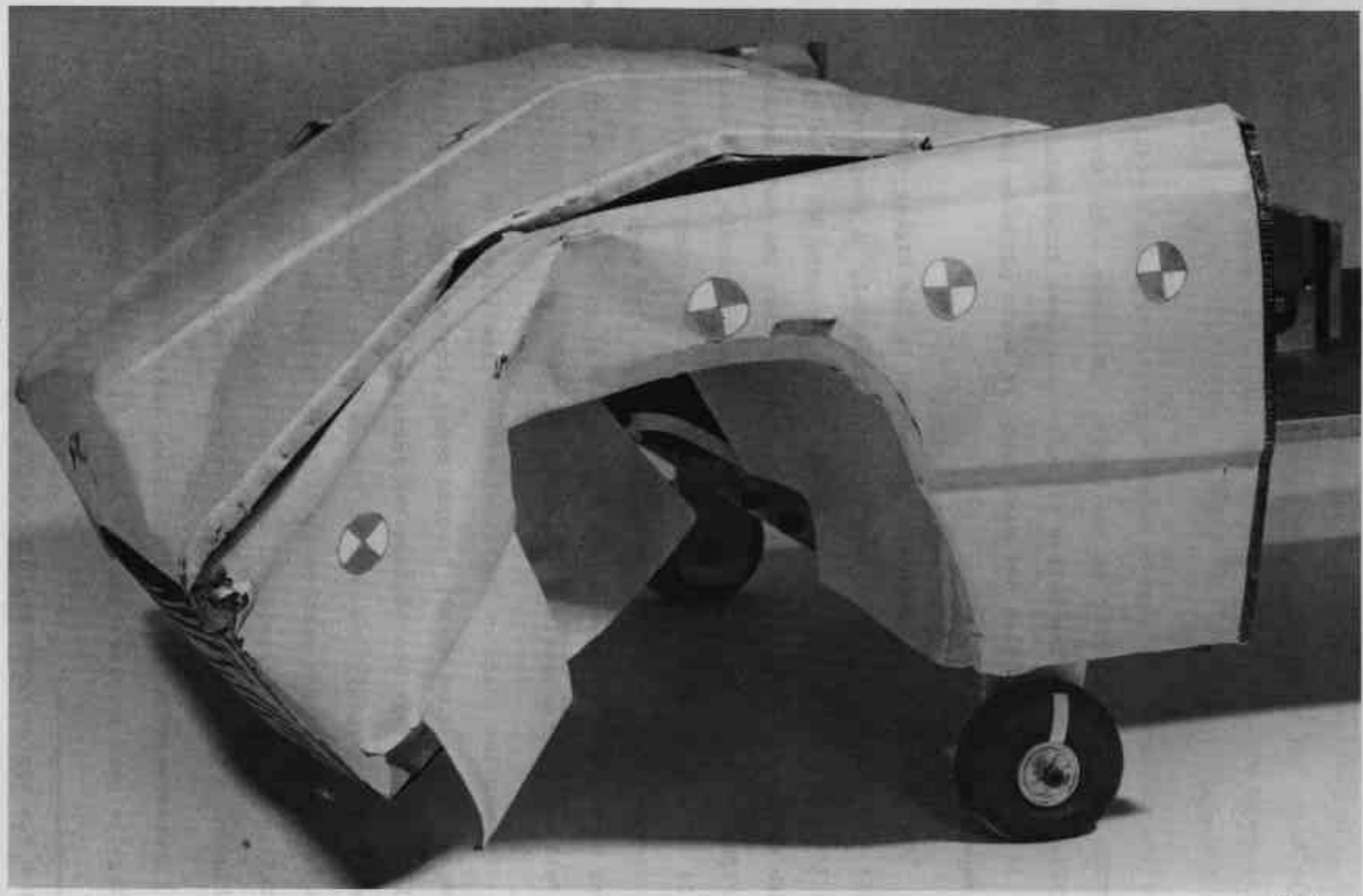

MP-3578-38

FIGURE 30 1/5-SCALE MODEL AFTER 20-mph BARRIER IMPACT

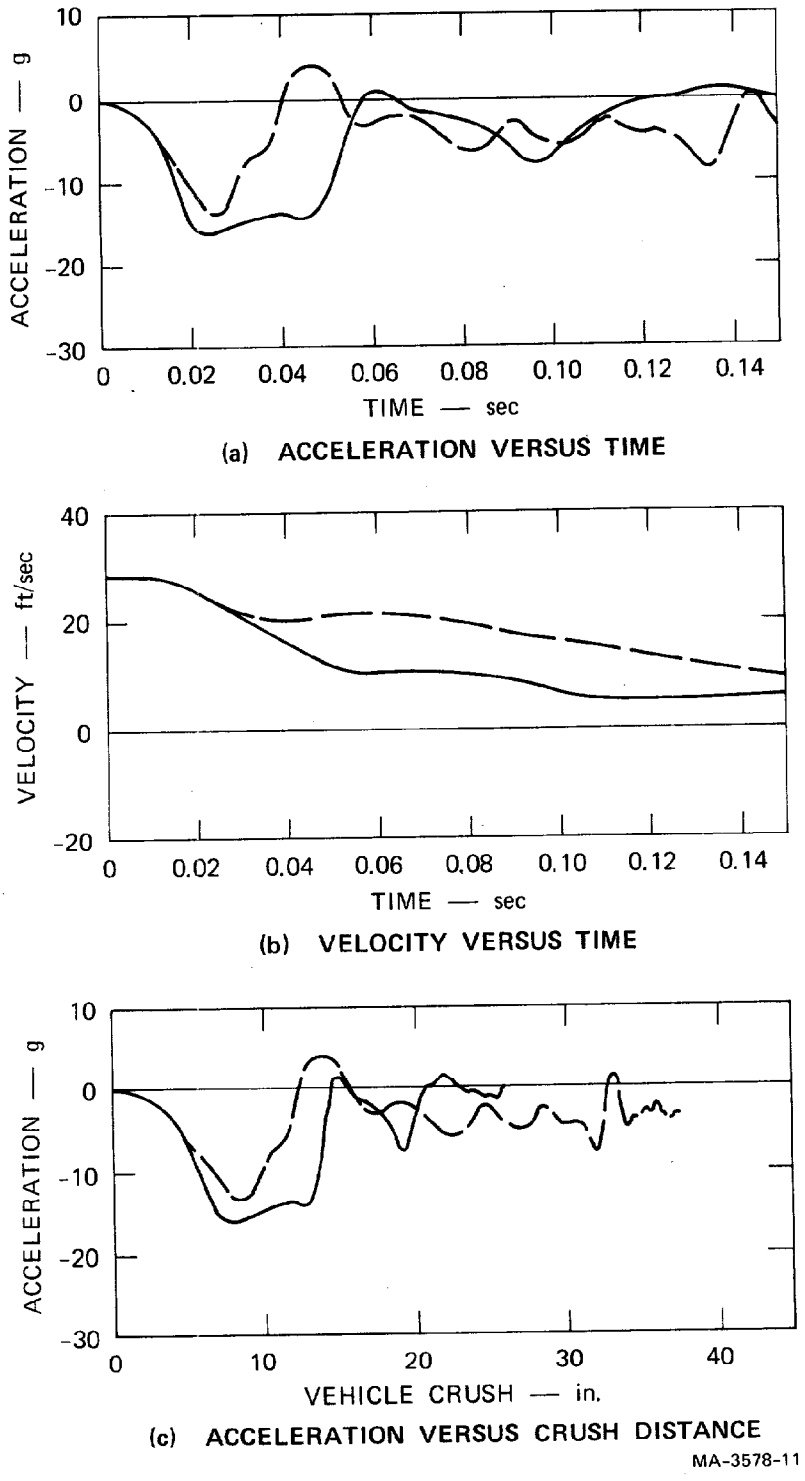

FIGURE 31 COMPARISON OF LONGITUDINAL ACCELERATION DATA FROM FULL-SCALE (— —) AND 1/5-SCALE (——) SHEET METAL EXPERIMENTS

the area under the curves in Figure 31(c), and the total crush from Figure 31(c). The peak acceleration in the full-scale test was 14 g, and the peak acceleration in the model test was 16 g, a difference* of 13 percent. The difference in energy absorption is 5 percent, and the difference in crush is 40 percent. The large difference in crush and the small difference in the other quantities indicates the difficulty in defining test accuracy. This problem will be addressed more completely in the final report.

Cost Summary

The 1/5-scale model test was used to provide detailed cost estimates for modeling automotive sheet metal structures. Costs obtained for each phase of model construction and testing are given in Table 5. These costs are applicable to any 1/5-scale model requiring five to seven large explosively formed parts. The total cost of the first model test was $8,300, but $4,500 of this is the cost of making the dies for the explosive forming process. The cost of later tests was lower ($3,500) because the dies were already made and the test shots needed to find the proper explosive charge had been conducted for the first test.

*Difference is defined as the 1/5-scale result minus the full-scale result divided by the average.

Table 5

TEST COSTS FOR MODELS WITH EXTENSIVE SHEET METAL

Item	First Test	Later Tests
Hand forming wooden punches	$3,000	--
Casting and machining aluminum dies	1,500	--
Explosive forming	1,500	$1,200
Vehicle fabrication	1,500	1,500
Test performance	800	800
Total	$8,300	$3,500

Appendix A

COMPAT: COMPUTER PROGRAM FOR LUMPED MASS ANALYSIS OF IN-LINE IMPACTS

COMPAT is a numerical integration routine that is designed to solve a specific problem, the collision of two automobiles represented as a system of masses connected by nonlinear springs. Each vehicle is made up of 6 masses (including one for the occupant) and 20 springs (as shown in Figure A-1). Note that the front facing in Vehicle 2 is redundant with that of Vehicle 1 and is omitted.

The governing equations for the mass-spring system are of the form

$$m_i \ddot{x}_i = F_j \tag{A-1}$$

where $m_i \ddot{x}_i$ is the product of the mass and acceleration of the i th mass and F_j is the sum of all the spring forces acting on that mass. The F_j are functions of the relative displacements (y) and velocities ($\dot{y}$) of the masses:

$$F_j = F_j(y_i, \dot{y}_i) \tag{A-2}$$

The force-deflection characteristics of the springs are specified by the user, but the general form of the force-deflection curves are built into the program as shown in Figure A-2. The user specifies the static force-deflection curve with a series of coordinates (up to 30) that give a piecewise linear approximation to the actual curve. The coordinates must lie in the 1st and 3rd quadrants or on the horizontal axis. The user also specifies the unloading slope S, which must be

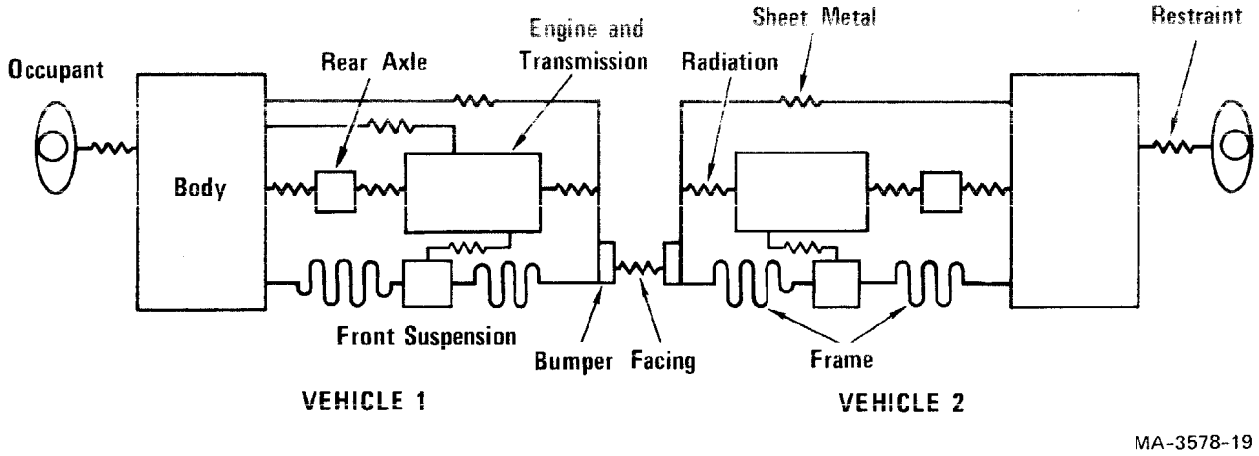

FIGURE A-1 IN-LINE IMPACT MODEL REPRESENTING VEHICLES AS A SYSTEM OF MASSES CONNECTED BY NONLINEAR SPRINGS

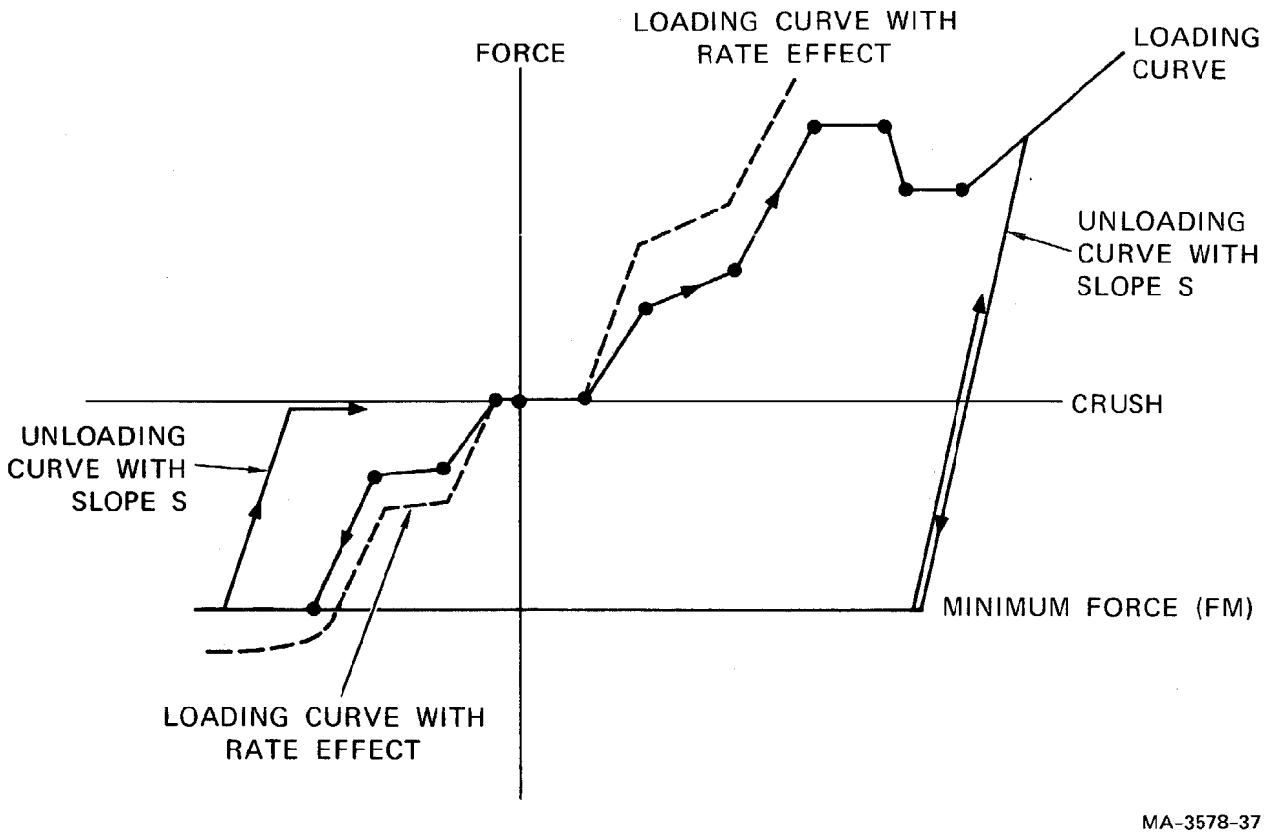

FIGURE A-2 FORCE-DEFLECTION CURVES

greater than any positive slope on the loading curve, and the minimum force, which must be zero or negative. Note that the minimum forces limit the force-deflection curve in the 3rd quadrant.

Rate effects are included in two ways: first, through a constant R, which is used with the static force FS obtained from the force deflection curve and the strain rate, or crush rate, $\dot{y}$ to obtain the dynamic force F,

$$F = FS(1 + R|\dot{y}|) \tag{A-3}$$

and second from a simple damper used in parallel with the nonlinear spring. It is specified by RL in lbf/ft/sec, so in general

$$F = FS(1 + R|\dot{y}|) + R2\ \dot{y} \tag{A-4}$$

Programming

COMPAT is written in FORTRAN IV extended and consists of a main program with subroutines. The subroutines and their functions are listed below:

HPCG--An integrator using Hamming's modified predictor-corrector method for solution of initial-value problems. HPCG was written by IBM. This subroutine uses a variable time step to keep errors within a specified tolerance.

RKGS--An integrator using a fourth-order Runge-Kutta method. This routine was also written by IBM and also incorporates a variable time step for error control.

FCT--This subroutine calculates the right-hand sides of the system of equations being integrated by HPCG or RKGS. The force-deflection characteristics of the springs are calculated here.

OUTP--This subroutine handles all output during integration.

OUTGR--This subroutine graphs parameters after integration is complete. The graph routine is unique to SRI.

Operation of COMPAT proceeds as follows: The initial values of velocities and displacements, force deflection curves, etc., are read into the program and printed. Then integration of the governing equations is turned over to HPCG or RKGS. The integrator then integrates the equations calling FCT and OUTP as required until the independent variable time reaches a preset value. Finally OUTGR plots any graphs desired.

Appendix B

COMPUTER INPUT FOR COMPAT

This appendix presents the input for COMPAT, a computer program for lumped mass analysis of in-line impacts. Two sets of inputs are given for each of the vehicles studied: first, the mass and location of the six components of the vehicle, and second, the piecewise linear representation of the nonlinear springs connecting these components. Inputs are given for the Calspan full size car, the AMF compact car, the Minicars and SRI subcompact cars, and the SRI full size car.

CALSPAN FULL SIZE CAR

MASS AND LOCATION

Component	Mass (lbm)	Distance to Front Interface at Impact (ft)
Bumper	50	0.3
Engine and transmission	900	2.6
Front suspension	250	3.6
Rear axle	250	13.6
Body	3050	5.3
Occupant	160	8.0
Total mass	4660	

PIECEWISE LINEAR REPRESENTATION OF SPRING CHARACTERISTICS

1. Front Facing

Crush (ft)	Force (kip)
-1.00	-100.0
0.00	0.0
0.10	500.0
0.30	1000.0
1.00	1000.0

FM = 100.0 kip
S = 5×10^6 lbf/ft
R = 0.0 sec/ft
R2 = 1.0×10^4 kip-sec/ft

2. Radiator

Crush (ft)	Force (kip)
-1.00	0.0
1.40	0.0
1.50	150.0
2.20	150.0
2.60	1.0×10^6
3.00	1.0×10^6

FM = 0.0
S = 1.0×10^8
R = 0.0
R2 = 0.0

3. Sheet Metal

Crush (ft)	Force (kip)
-1.00	0.0
0.50	0.0
0.70	23.0
1.20	15.0
2.40	17.0
3.40	55.0
5.00	55.0

FM = 0.0
S = 5.0×10^6
R = 0.0
R2 = 0.0

4. Forward Frame	
Crush (ft)	Force (kip)
-1.00	0.0
0.00	0.0
0.01	16.0
0.25	16.0
0.30	75.0
0.55	55.0
1.00	30.0
4.00	30.0

FM = 0.0
S = 5×10^6
R = 0.03
R2 = 0.0

5. Motor Mount	
Crush (ft)	Force (kip)
-1.67	-20.0
-0.17	-20.0
-0.08	-10.0
0.00	0.0
0.08	10.0
0.17	20.0
1.67	20.0

FM = -1.0
S = 2×10^5
R = 0.0
R2 = 0.0

6. Aft Frame	
Crush (ft)	Force (kip)
-1.00	0.0
0.00	0.0
0.05	75.0
0.30	55.0
0.75	30.0
4.00	30.0
4.10	30.0

FM = 0.0
S = 5×10^6
R = 0.03
R2 = 0.0

7. Drive Shaft	
Crush (ft)	Force (kip)
-2.00	0.0
0.00	0.0
0.10	15.0
0.20	17.0
0.30	0.0
3.00	0.0

FM = 0.0
S = 5×10^6
R = 0.0
R2 = 0.0

8. Rear Suspension	
Crush (ft)	Force (kip)
-1.00	-17.0
-0.83	-17.0
0.00	0.0
0.58	30.0
0.60	20.0
4.00	20.0

FM = -10.0
S = 2×10^6
R = 0.0
R2 = 0.0

9. Firewall	
Crush (ft)	Force (kip)
-3.00	0.0
0.05	0.0
0.55	100.0
1.50	25.0
3.00	10.0

FM = 0.0
S = 1.0×10^6
R = 0.0
R2 = 0.0

AMF COMPACT CAR

MASS AND LOCATION

Component	Mass (lbm)	Distance to Front Interface at Impact (ft)
Bumper	50	0.3
Engine and transmission	675	1.4
Front suspension	423	3.0
Rear axle	200	11.8
Body	1632	4.5
Occupant	160	8.8
Total mass	3140	

PIECEWISE LINEAR REPRESENTATION OF SPRING CHARACTERISTICS

1. Front Facing

Crush (ft)	Force (kip)
-1.60	0.0
0.00	0.0
0.04	29.0
0.29	60.0
0.34	26.0
0.84	75.0

FM = 0.0 kip
S = 1.0×10^5 lbf/ft
R = 0.0 sec/ft
R2 = 6×10^3 kip-sec/ft

2. Radiator

Crush (ft)	Force (kip)
-4.17	0.0
1.04	0.0
1.21	2.3
1.38	6.2
1.54	10.7
1.79	26.5
1.92	62.3
1.93	120.0
2.38	500.0

FM = 0.0
S = 8.0×10^5
R = 0.0
R2 = 0.0

3. Sheet Metal

Crush (ft)	Force (kip)
-4.17	0.0
0.00	0.0
0.08	17.0
0.29	17.0
0.33	7.0
7.83	7.0

FM = 0.0
S = 2.0×10^5
R = 0.0
R2 = 0.0

4. Forward Frame	
Crush (ft)	Force (kip)
-4.17	0.0
0.00	0.0
0.08	40.0
0.25	60.0
0.29	75.0
0.42	60.0
1.50	50.0
1.58	100.0
4.17	100.0

FM = 0.0
S = 6.0×10^5
R = 0.01
R2 = 0.0

5. Motor Mount	
Crush (ft)	Force (kip)
-1.67	-20.0
-0.17	-20.0
-0.08	-10.0
0.00	0.0
0.08	10.0
0.17	20.0
1.67	20.0

FM = -20.0
S = 1.2×10^5
R = 0.0
R2 = 0.0

6. Aft Frame	
Crush (ft)	Force (kip)
-0.83	-60.0
0.08	-50.0
0.00	0.0
0.08	50.0
0.33	75.0
0.83	35.0
0.92	80.0
2.50	80.0

FM = -70.0
S = 5.0×10^5
R = 0.01
R2 = 0.0

7. Drive Shaft	
Crush (ft)	Force (kip)
-0.83	-5.0
0.00	0.0
0.16	12.3
0.59	15.1
0.88	4.7
1.03	4.7
1.12	0.0
4.17	0.0

FM = -5.0
S = 8.0×10^4
R = 0.0
R2 = 0.0

8. Rear Suspension	
Crush (ft)	Force (kip)
-2.00	-100.0
-1.00	-100.0
1.00	100.0
2.00	100.0

FM = -100.0
S = 1.0×10^5
R = 0.0
R2 = 0.0

9. Firewall	
Crush (ft)	Force (kip)
-0.83	0.0
0.13	0.0
0.15	4.0
0.23	4.0
0.43	10.0
0.53	10.0
0.60	11.0
0.73	11.0
0.84	15.4
0.99	14.7
1.46	16.3
4.17	16.3

FM = -16.0
S = 2.0×10^4
R = 0.0
R2 = 0.0

MINICARS AND SRI SUBCOMPACT CARS

MASS AND LOCATION

Component	Mass (lbm)	Distance to Front Interface at Impact (ft)
Bumper	50	0.3
Engine and transmission	426	2.5
Front suspension	162	3.65
Rear axle	202	12.5
Body	1715	6.0
Occupant	160	8.0
Total mass	2715	

PIECEWISE LINEAR REPRESENTATION OF SPRING CHARACTERISTICS

1. Front Facing

Crush (ft)	Force (kip)
-1.00	-100.0
0.00	0.0
0.10	500.0
0.30	1000.0
1.00	1000.0

FM = 100.0 kip
S = 5.0×10^6
R = 0.0 sec/ft
R2 = 6.0×10^3 kip-sec/ft

2. Radiator

Crush (ft)	Force (kip)
-1.00	0.0
1.58	0.0
1.66	2.0
1.81	6.0
1.91	10.0
2.00	19.0
2.08	27.0
2.16	35.0
2.33	50.0
2.50	1.0×10^6

FM = 0.0
S = 1.0×10^8
R = 0.0
R2 = 0.0

3. Sheet Metal

Crush (ft)	Force (kip)
-1.00	0.0
0.75	0.0
2.00	35.0
5.00	35.0
5.50	100.0

FM = 0.0
S = 5.0×10^6
R = 0.0
R2 = 0.0

4. Forward Frame

Crush (ft)	Force (kip)
-1.00	-10.0
0.00	0.0
0.01	18.0
0.50	18.0
0.55	24.0
2.50	24.0
3.00	100.0
3.10	1000.0

FM = -100.0
S = 5.0×10^6
R = 0.0
R2 = 0.0

5. Motor Mount

Crush (ft)	Force (kip)
-1.00	-5.5
-0.42	-5.5
-0.25	-2.0
-0.10	-2.0
0.00	0.0
0.33	9.0
0.67	16.0
0.92	16.0
1.00	10.0
1.17	12.0
5.00	1.0

FM = -5.5
S = 5.0×10^4
R = 0.0
R2 = 0.0

6. Aft Frame

Crush (ft)	Force (kip)
-1.00	-10.0
0.00	0.0
0.01	24.0
1.00	24.0
1.50	100.0
2.00	1000.0

FM = -10.0
S = 5.0×10^6
R = 0.0
R2 = 0.0

7. Drive Shaft

Crush (ft)	Force (kip)
-1.00	0.0
2.00	0.0
2.50	100.0
4.00	100.0

FM = 0.0
S = 5.0×10^6
R = 0.0
F2 = 0.0

8. Rear Suspension

Crush (ft)	Force (kip)
-1.00	-10.0
-0.83	-10.0
0.00	0.0
0.58	17.0
0.60	11.0
4.00	11.0

FM = -10.0
S = 2.0×10^6
R = 0.0
R2 = 0.0

9. Firewall

Crush (ft)	Force (kip)
-1.00	0.0
5.00	0.0

FM = 0.0
S = 1.0×10^6
R - 0.0
R2 = 0.0

SRI FULL SIZE CAR

MASS AND LOCATION

Component	Mass (lbm)	Distance to Front Interface at Impact (ft)
Bumper	50	0.3
Engine and transmission	900	2.9
Front suspension	250	3.95
Rear axle	250	13.6
Body	3050	5.6
Occupant	160	7.3
Total mass	4660	

PIECEWISE LINEAR REPRESENTATION OF SPRING CHARACTERISTICS

1. Front Facing

Crush (ft)	Force (kip)
-1.00	-100.0
0.00	0.0
0.10	500.0
0.30	1000.0
1.00	1000.0

FM = -100.0 kip
S = 5.0×10^6 lbf/ft
R = 0.0 sec/ft
R2 = 6.0×10^3 kip-sec/ft

2. Radiator

Crush (ft)	Force (kip)
-1.00	0.0
1.90	0.0
2.00	150.0
2.50	150.0
2.60	1.0×10^6
3.00	1.0×10^6

FM = 0.0
S = 1.0×10^8
R = 0.0
R2 = 0.0

3. Sheet Metal

Crush (ft)	Force (kip)
-1.00	0.0
0.50	0.0
0.60	40.0
1.50	40.0
2.00	50.0
2.20	100.0
3.00	100.0
4.50	125.0

RM = 0.0
S = 5.0×10^6
R = 0.0
R2 = 0.0

4. Forward Frame	
Crush (ft)	Force (kip)
-1.00	-10.0
0.00	0.0
0.01	18.0
0.50	18.0
0.55	24.0
2.50	24.0
3.00	100.0
3.10	1000.0
FM = -100.0	
S = 5.0×10^6	
R = 0.0	
R2 = 0.0	

5. Motor Mount	
Crush (ft)	Force (kip)
-5.0	0.0
5.0	0.0
RM = 0.0	
S = 5.0×10^4	
R = 0.0	
R2 = 0.0	

6. Aft Frame	
Crush (ft)	Force (kip)
-1.00	-10.0
0.00	0.0
0.01	24.0
1.00	24.0
1.50	100.0
2.00	1000.0
FM = -10.0	
S = 5.0×10^6	
R = 0.0	
R2 = 0.0	

7. Drive Shaft	
Crush (ft)	Force (kip)
-2.00	0.0
0.00	0.0
0.10	15.0
0.20	17.0
0.30	0.0
3.00	0.0
FM = 0.0	
S = 5.0×10^6	
R = 0.0	
R2 = 0.0	

8. Rear Suspension	
Crush (ft)	Force (kip)
-1.00	-17.0
0.83	-17.0
0.00	0.0
0.58	30.0
0.60	20.0
4.00	20.0
RM = -10.0	
S = 2.0×10^6	
R = 0.0	
R2 = 0.0	

9. Firewall	
Crush (ft)	Force (kip)
-1.00	0.0
0.75	0.0
1.75	30.0
2.25	50.0
2.50	100.0
3.00	100.0
FM = 0.0	
S = 1.0×10^6	
R = 0.0	
R2 = 0.0	